



**HAL**  
open science

## Postrift history of the eastern central Atlantic passive margin: Insights from the Saharan region of South Morocco

Rémi Leprêtre, Yves Missenard, Jocelyn Barbarand, Cécile Gautheron, Omar Saddiqi, Rosella Pinna-Jamme

► **To cite this version:**

Rémi Leprêtre, Yves Missenard, Jocelyn Barbarand, Cécile Gautheron, Omar Saddiqi, et al.. Postrift history of the eastern central Atlantic passive margin: Insights from the Saharan region of South Morocco. *Journal of Geophysical Research: Solid Earth*, 2015, 120 (6), pp.4645-4666. 10.1002/2014JB011549 . hal-03951492

**HAL Id: hal-03951492**

**<https://hal.science/hal-03951492>**

Submitted on 23 Jan 2023

**HAL** is a multi-disciplinary open access archive for the deposit and dissemination of scientific research documents, whether they are published or not. The documents may come from teaching and research institutions in France or abroad, or from public or private research centers.

L'archive ouverte pluridisciplinaire **HAL**, est destinée au dépôt et à la diffusion de documents scientifiques de niveau recherche, publiés ou non, émanant des établissements d'enseignement et de recherche français ou étrangers, des laboratoires publics ou privés.

## RESEARCH ARTICLE

10.1002/2014JB011549

## Key Points:

- South Moroccan passive margin has a polyphased Mesozoic-Cenozoic thermal history
- An early postrift event controls the topographic evolution of the whole margin
- Lithospheric structure and rifting process control the early margin topography

## Supporting Information:

- Texts S1 and S2, Figures S1–S12, and Tables S1–S5

## Correspondence to:

R. Leprêtre,  
remi.lepretre@u-psud.fr

## Citation:

Leprêtre, R., Y. Missenard, J. Barbarand, C. Gautheron, O. Saddiqi, and R. Pinna-Jamme (2015), Postrift history of the eastern central Atlantic passive margin: Insights from the Saharan region of South Morocco, *J. Geophys. Res. Solid Earth*, 120, 4645–4666, doi:10.1002/2014JB011549.

Received 19 AUG 2014

Accepted 14 MAY 2015

Accepted article online 19 MAY 2015

Published online 29 JUN 2015

## Postrift history of the eastern central Atlantic passive margin: Insights from the Saharan region of South Morocco

Rémi Leprêtre<sup>1</sup>, Yves Missenard<sup>1</sup>, Jocelyn Barbarand<sup>1</sup>, Cécile Gautheron<sup>1</sup>, Omar Saddiqi<sup>2</sup>, and Rosella Pinna-Jamme<sup>1</sup>

<sup>1</sup>GEOPS, Université Paris Sud-11, Orsay, France, <sup>2</sup>Geosciences, Université Hassan II, Casablanca, Morocco

**Abstract** The passive margin of South Morocco is a low-elevated passive margin. It constitutes one of the oldest margins of the Atlantic Ocean, with an Early Jurassic breakup, and little geological data are available concerning its postrift reactivation so far. We investigated the postrift thermal history of the onshore part of the margin with low-temperature thermochronology on apatite crystals. Fission track and (U-Th-Sm)/He ages we obtained are significantly younger than the breakup (~190 Ma). Fission track ages range from  $107 \pm 8$  to  $175 \pm 16$  Ma, with mean track lengths from  $10.7 \pm 0.3$  to  $12.5 \pm 0.2$   $\mu\text{m}$ . (U-Th-Sm)/He ages range from  $14 \pm 1$  to  $185 \pm 15$  Ma. Using inverse modeling of low-temperature thermochronological data, we demonstrate that the South Moroccan continental margin underwent a complex postrift history with at least two burial and exhumation phases. The first exhumation event occurred during Late Jurassic/Early Cretaceous, and we attribute this to mantle dynamics rather than to intrinsic rifting-related processes such as flexural rebound. The second event, from Late Cretaceous to early Paleogene, might record the onset of Africa/Europe convergence. We show a remarkably common behavior of the whole Moroccan passive margin during its early postrift evolution. The present-day differences result from a segmentation of the margin domains due to the Africa/Europe convergence. Finally we propose that varying retained strengths during rifting and also the specific crustal/lithospheric geometry of stretching explain the difference between the topographical expressions on the continental African margin compared to its American counterpart.

### 1. Introduction

The so-called “passive” margins are characterized by complex postrift evolutions. Vertical motions that clearly postdate the rifting have indeed been identified in many geological settings: Greenland [Johnson and Gallagher, 2000; Japsen et al., 2014; Bonow et al., 2014], the eastern North Atlantic realm [Holford et al., 2009], Brazil [Harman et al., 1998; Cogné et al., 2012], eastern North America [Pazzaglia and Gardner, 1994], South Africa [Turner et al., 2008; Brown et al., 2002, 2014], and Northwest Africa [Sahagian, 1988; Roberts and White, 2010; Beauvais and Chardon, 2013]. Almost all these studies were carried out on high-elevated passive margins. This link between actual high-elevated topography and postrift motions specifically questions whether or not these motions can be responsible for the current high topography of many passive margins [Japsen et al., 2012].

Low-elevated passive margins have received little attention compared to high-elevated ones [Bishop, 2007] given the geomorphological issue regarding the latter. In this study, we focus our attention on the low-elevated passive margin of South Morocco (Figures 1a, 1b, and 2), which results from the breakup of the central Atlantic Ocean during the Lower Jurassic at circa 190 Ma [Labails et al., 2010]. Here the Precambrian cratonic lithosphere of the West African Craton (WAC) abuts the oceanic Atlantic lithosphere. This cratonic lithosphere is considered quite stable, and it is unlikely that this lithosphere has undergone large amplitude motions. Nevertheless, there is indirect evidence of postrift uplift of the margin. Together, the presence of forced regression prisms during the Early Cretaceous at the slope of the West African margin [Mitchum and Vail, 1977] and Cenomanian-Turonian marine deposits at relatively high elevations [Sahagian, 1988] around the Anti-Atlas and in the western Tindouf Basin (up to more than 1 km and 500 m high, respectively), which are far beyond the maximum eustatic amplitudes ( $\pm 100$  m), suggest significant postrift vertical motions of the onshore continental margin. This scattered evidence clearly indicates postrift movements whose precise timing still has to be established in order to thoroughly understand the postrift evolution of the margin.

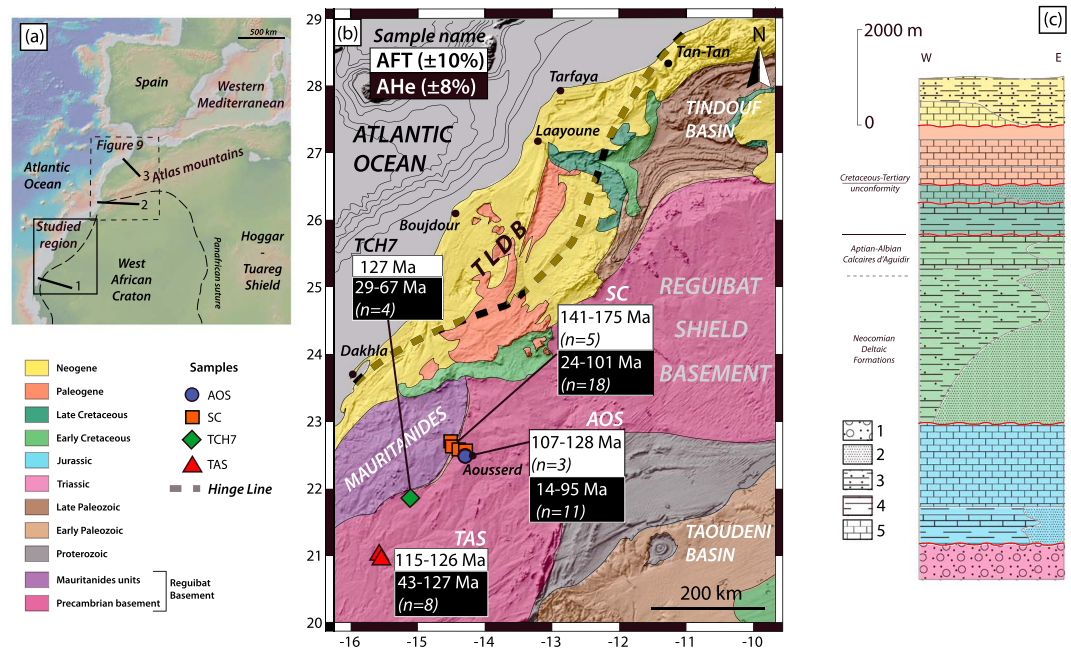


**Figure 1.** (a) Geographical map the eastern central Atlantic Ocean and western Mediterranean. It locates the studied region shown in Figure 1b, Figure 9, and Figure 3 topographic profiles along the passive margin of Morocco (presented in Figures 2 and 9). (b) Geological map of the studied area. The bathymetry (isobaths are 500 m spaced from the coast) is also presented to see how the platform extends seaward. The hinge line represents the limit of crustal thinning due to the rifting (see seismic profile in *Labails et al.* [2009] for its specific position at the Dakhla latitude). For the rest of the margin, we used the hinge line as defined in *von Rad et al.* [1982]. The Mauritanides are a part of the basement of the Reguibat Shield. The shield was structured during the Pan-African orogeny [*Villeneuve, 2008*]. LT thermochronology results are incorporated and grouped as indicated in the text (section 3.2) with colored labels. The variable *n* precises the number of thermochronological data, i.e., the number of analyzed grains for AHe methodology and the number of samples for AFT methodology (see Tables 1 and 2 for details). TLDB: Tarfaya-Laayoune-Dakhla Basin. (c) Stratigraphical log of the onshore northern TLDB [after *Ranke et al., 1982*]. This is the most complete sedimentary succession, since the Late Cretaceous, and maybe parts of the upper section of the Early Cretaceous are eroded south of 24°N. Colors are the same than used for Figure 1b. 1 = conglomerates and coarse detrital sediments; 2 = coarse to fine sandstones; 3 = shales with variable sandy proportion; 4 = Shales and clays, sometimes interbedded with limestones; 5 = limestones.

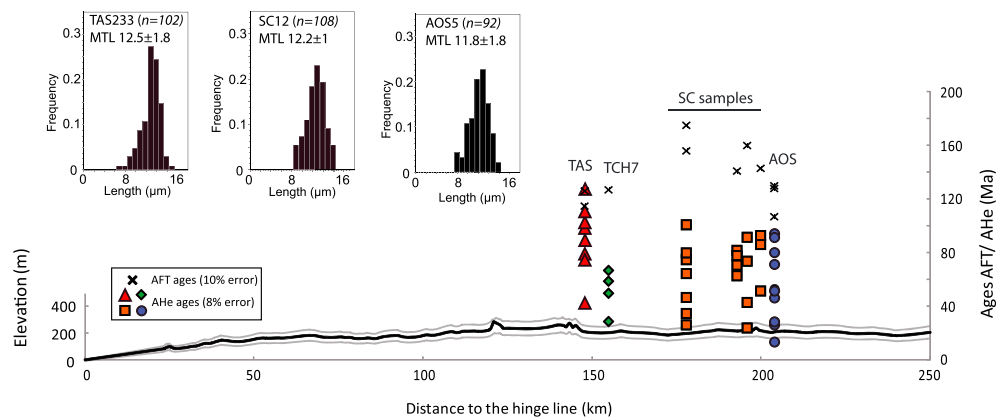


**Figure 2.** Cross section of the onshore margin (profile 1 in Figure 1b) with geographical distribution of the thermochronological data (AFT and corrected AHe ages). Same legend as in Figure 1 for each sample. The locations of the various sampling sites are projected along a section perpendicular to the coast. The fission track lengths data are given for three representative samples TAS233, SC12, and AOS5 given they provided sufficient lengths to measure. Other samples from SC and AOS groups show similar length distributions, whereas we did not use length distribution for TCH7 as it carried too few (*n* = 37). Light grey lines show the maximum variation in elevation within 50 km from the main cross section (black line).

We thus led the first low-temperature thermochronology in this area, coupling fission track and (U-Th)/He dating on apatite (apatite fission track (AFT) and AHe dating, respectively). These low-temperature thermochronometers have a 50–120°C temperature range sensitivity [Gallagher *et al.*, 1998; Flowers *et al.*, 2009; Gautheron *et al.*, 2009] and allow modeling of the thermal history of the 3–4 km of the upper crust of the onshore basement of the margin using forward and inverse modeling. The combined interest of AFT and AHe methods allows us to determine more refined thermal histories than using one or the other method alone, though it is still not routinely used for the study of passive margins (see examples of combined use in Persano *et al.* [2002] and Cogné *et al.* [2012]). Thermal histories with alternating cooling and heating phases are translated into a succession of exhumation and burial phases and coupled with the stratigraphical record to provide insight into the evolution of the margin.

We propose the first comprehensive geological history in this domain, revealing a polyphased burial/exhumation history for the onshore margin basement. We conduct a comparison with the other segments of the Moroccan passive margin so as to ascertain the global evolution of this moderate to low-lying passive margin. Finally, we make a comparison between the Moroccan passive margin and its conjugate passive margin in Northeast America in order to question the mechanisms which caused the different early postrift evolutions.

## 2. Geological Setting

The passive margin of the eastern central Atlantic comprises the narrow Tarfaya-Laayoune-Dakhla Basin, bounded to the east and south by the basement of the western Reguibat Shield (Figure 1b). The Reguibat Shield belongs to the West African Craton (WAC) [Ennih and Liégeois, 2008; Youbi *et al.*, 2013], which dates from Archean to Early Proterozoic for the Reguibat Shield basement [Potrel *et al.*, 1996; Montero *et al.*, 2014]. In the past 600 Ma, this region has been involved in major tectonic events during two orogenic cycles, the Pan-African and the Variscan ones, which set up the Mauritanides nappes [Villeneuve, 2008; Michard *et al.*, 2010] (Figure 1b), and the subsequent rifting/breakup during the Atlantic opening, focusing on inherited weakened zones [Villeneuve and Marcaillou, 2013]. The Reguibat Shield is also bounded by Precambrian and Paleozoic basins on its southern and northern borders (Taoudeni and Tindouf basins, respectively).

The Tarfaya-Laayoune-Dakhla Basin (TLDB; Figures 1b and 1c) is a NE-SW oriented basin, resulting from the opening of the central Atlantic. The timing of the central Atlantic Ocean opening has recently been revised by Labails *et al.* [2010] who estimate the breakup age in the Late Sinemurian (190 Ma). The margin represents a 100 km wide thinned domain, the crust thickness evolving from 27 km to 7 km [Klingelhoefer *et al.*, 2009]. This stretched domain is filled by more than 10 km of sediments (maximum of 14 km) from Triassic to the present day [Ranke *et al.*, 1982], and the sedimentary infill thins eastward up to its disappearance on the western Reguibat Shield basement (Figure 1b). Its stratigraphy and geometry are known from the various drills from oil exploration [AUXINI, 1969] and a few seismic sections [Mitchum and Vail, 1977; El Khatib, 1995; Davison, 2005; Hafid *et al.*, 2008; Labails *et al.*, 2009], Deep Sea Drilling Project reports (139, 369, and 197) and field studies [Choubert *et al.*, 1966; Martinis and Visintin, 1966; Ratschiller, 1968].

The Mesozoic-Cenozoic regional stratigraphy of the onshore and offshore parts of the TLDB has been summarized by Ranke *et al.* [1982]. The onshore stratigraphy is presented in Figure 1c. Triassic formations (sandstones, conglomerates, volcanic rocks, and evaporites) lie unconformably on the basement. Directly above it, the Jurassic shows the buildup of a large carbonate platform, mostly during the Middle to Late Jurassic/Berriasian. An abrupt change is recorded at the beginning of the Early Cretaceous (Neocomian-Barremian), with deposition of detrital formations. Huge volume of continental clastics in the Early Cretaceous marked the drowning of the platform and the formation of immense prograding deltas at the latitude of TanTan/Tarfaya and Boujdour [Ratschiller, 1968; Ranke *et al.*, 1982]. The Lower Cretaceous formations lie unconformably on top of the older ones and even on the basement in the east (Figure 1b). Marine conditions resume in Aptian-Albian times with the deposition of carbonate beds [Martinis and Visintin, 1966] and, in the offshore domain, the landward migration of detrital facies [Einsele and von Rad, 1979]. The thickness of the Aptian-Albian formations is variable and can reach at least 1 km, even close to the Reguibat Shield [AUXINI, 1969]. The high-stand sea level at the beginning of the

Late Cretaceous (Cenomanian-Turonian) is well expressed, in the northern TLDB, with the deposition of unconformable black shale and carbonates in a context of increasing water depths [Sachse *et al.*, 2011]. Erosion has recently erased a large part of the traces of the Late Cretaceous in the offshore northern TLDB [Ranke *et al.*, 1982]. The early terms of Paleogene are still marine but representative of shallower depths and, in some places, show clastics (e.g., in the Tarfaya subbasin). The generalized decreasing sea level leads to the deposition of Eocene clastics. Paleocene and Eocene formations lie unconformably on the Late Cretaceous in the north of the basin, and on the Early Cretaceous south of Boujdour. There is no Oligocene formation in the onshore domain of the TLDB. Neogene deposits are scarce and thin on the onshore TLDB [Ranke *et al.*, 1982], except in a small basin near Laayoune, where marine deposits reach 1000 m.

### 3. Methodology

#### 3.1. Sampling

Sampling perpendicular to the margin has been taken following the road that goes across the Reguibat Shield, toward the Aousserd syenite (Figures 1 and 2). Eleven samples were collected from the basement: three of them come from the ~2.5 Ga Aousserd syenite [Bea *et al.*, 2013] (AOS samples), five samples come from the metamorphic Mauritanides (SC samples) that reworked Pan-African rocks [Michard *et al.*, 2010], one from the Tichla gabbro massif (south of the Mauritanides, probably Archean in age; TCH7 sample), and the two last are gneisses from the Tasiast basement formations, Mauritania (~2.8 Ga [Chardon, 1997]; TAS samples). Detrital Cretaceous formations of the southern TLDB have been sampled but did not yield any apatites for AFT and AHe analysis.

#### 3.2. Low-Temperature Thermochronology

Low-temperature (LT) thermochronology with AFT and AHe dating was carried out at the Geosciences Paris Sud (GEOPS) laboratory (Université Paris Sud-11, Orsay, France). Samples were crushed and sieved, and apatite crystals were separated with heavy liquors/magnetic separation and handpicking. Ten samples with sufficient apatite crystals have been selected for the AFT methodology. Within these, nine samples allowed AHe dating.

AFT dating was carried out using the external detector method [Gleadow and Duddy, 1981]. We used the central age method [Galbraith and Laslett, 1993] with a zeta [Hurford and Green, 1983] of  $368 \pm 10$  (R. Leprêtre) determined with a CN5 glass dosimeter and Durango/Fish Canyon apatite standards [Hurford, 1990]. Spontaneous tracks were revealed by etching in 5 M HNO<sub>3</sub> for 20 s at  $20 \pm 1^\circ\text{C}$ . Dpar were also measured to check the chemical control on fission track annealing [Barbarand *et al.*, 2003]. Horizontal confined track lengths were measured using a LEICA light microscope with a X1000 magnification, and a digitizing tablet linked via a drawing tube to the microscope. AFT ages and lengths are given in Table 1 and Figures 2, 3, and S1 in the supporting information.

AHe analysis was carried out on euhedral inclusion-free apatite crystals with a minimum of three replicates per sample. Crystal dimensions and geometry were measured along the three axes and placed into a platinum basket. Ejection factors and sphere equivalent radius were determined using the Monte Carlo simulation from Ketcham *et al.* [2011]. More details on He, U, Th, and Sm content determination can be found in Gautheron *et al.* [2013]. The analysis was calibrated using internal and external age standards. Mean AHe ages of  $16.6 \pm 1.1$  Ma and  $31.8 \pm 0.5$  Ma have been measured for the Limberg tuff and Durango yellow apatite, which are in agreement with literature data (i.e.,  $16.8 \pm 1.1$  Ma from Kraml *et al.* [2006] and  $31.4 \pm 0.2$  Ma from McDowell *et al.* [2005]). The error on the AHe age at  $1\sigma$  is estimated to be a maximum of 8% reflecting uncertainty in the ejection factor ( $F_{\gamma}$ ) correction and standard dispersion. The final He, U-Th-Sm content, and AHe age are reported in Table 2.

Each apatite grain for a particular thermal history and crystal size is characterized by a different AHe closure temperature [Dodson, 1973], as the He diffusion coefficient evolves with the damage fraction [Shuster *et al.*, 2006; Shuster and Farley, 2009]. So scattered AHe ages emphasize the difference in AHe closure temperature for each grain coupled with a long stay in the He partial retention zone. This behavior has been incorporated into two predictive models, in which the radiation damage annealing is considered to follow annealing kinetics similar to fission tracks [Ketcham *et al.*, 2007; Gautheron *et al.*, 2009; Flowers *et al.*, 2009]. The observable variation in eU for various replicates (Figures 4 and S2) for the same sample is

Table 1. AFT Results<sup>a</sup>

Sample	Rock Type	Location	Elevation (m)	$\rho_s$ ( $10^6$ tr/cm <sup>2</sup> )	$\rho_i$ ( $10^6$ tr/cm <sup>2</sup> )	$\rho_d$ ( $10^6$ tr/cm <sup>2</sup> )	Central Age (Ma) $\pm 1\sigma$	$P$ ( $\chi^2$ ) (%)	$U$ (ppm)	MTL ( $\mu$ m) $\pm$ se	MTL Standard Deviation	Dpar
AOS2	neph. syen.	14°17'W 22°32'N	400	1.124 <i>654</i>	1.258 <i>732</i>	6.61 <i>6528</i>	107 $\pm$ 8 <i>21</i>	2	23	11.8 $\pm$ 0.2 <i>56</i>	1.8	1.7 $\pm$ 0.3
AOS3	neph. syen.	14°17'W 22°32'N	400	1.899 <i>1301</i>	1.772 <i>1241</i>	6.58 <i>6528</i>	128 $\pm$ 6 <i>21</i>	63	33	11.9 $\pm$ 0.2 <i>100</i>	1.6	1.7 $\pm$ 0.3
AOS5	neph. syen.	14°17'W 22°32'N	400	1.381 <i>1153</i>	1.308 <i>1092</i>	6.55 <i>6528</i>	128 $\pm$ 8 <i>21</i>	<1	24	11.8 $\pm$ 0.2 <i>92</i>	1.8	1.8 $\pm$ 0.3
SC11	granite	14°21'38"W 22°34'36"N	293	0.85 <i>604</i>	0.627 <i>446</i>	6.5 <i>6528</i>	160 $\pm$ 11 <i>21</i>	50	12	12.1 $\pm$ 0.3 <i>32</i>	1.8	1.8 $\pm$ 0.3
SC12	granite	14°23'00"W 22°35'14"N	292	1.383 <i>1094</i>	1.155 <i>914</i>	6.47 <i>6528</i>	141 $\pm$ 8 <i>21</i>	27	22	12.2 $\pm$ 0.2 <i>108</i>	1.8	1.5 $\pm$ 0.2
TCH7	granite	15° 6'37.25"W 21°50'54.88"N	194	0.955 <i>916</i>	0.889 <i>853</i>	6.52 <i>6528</i>	127 $\pm$ 8 <i>21</i>	27	17	9.4 $\pm$ 0.3 <i>37</i>	2	1.6 $\pm$ 0.4
SC5	granite	14°29'38.00"W 22°40'50.00"N	284	1.04 <i>1131</i>	0.839 <i>913</i>	6.657 <i>6563</i>	156 $\pm$ 15 <i>20</i>	<1	15	10.7 $\pm$ 0.3 <i>32</i>	1.7	1.6 $\pm$ 0.1
SC9	granite	14°18'56.00"W 22°33'8.00"N	318	1.742 <i>866</i>	1.549 <i>770</i>	6.641 <i>6563</i>	143 $\pm$ 13 <i>20</i>	<1	28	11.2 $\pm$ 0.3 <i>31</i>	1.9	1.7 $\pm$ 0.1
SC15	granite	14°28'52.00"W 22°40'17.00"N	282	0.6 <i>482</i>	0.425 <i>341</i>	6.626 <i>6563</i>	175 $\pm$ 16 <i>20</i>	10	8	- -	-	1.7 $\pm$ 0.1
TAS233	volcanite	15°32'55.96"W 20°59'34.10"N	110	0.68 <i>797</i>	0.651 <i>763</i>	6.634 <i>6849</i>	126 $\pm$ 7 <i>20</i>	87	12	12.5 $\pm$ 0.2 <i>102</i>	1.8	1.6 $\pm$ 0.2
TAS29	gneiss	15°32'55.96"W 20°59'34.10"N	110	0.743 <i>1047</i>	0.778 <i>1096</i>	6.586 <i>6849</i>	115 $\pm$ 6 <i>20</i>	11	14	12.2 $\pm$ 0.2 <i>51</i>	1.8	1.7 $\pm$ 0.1

<sup>a</sup>  $\rho_s$  = density of tracks with s and i = spontaneous and induced densities in apatites and the mica detector; d = tracks density of the neutron glass monitor (CN5);  $\rho_s$ ,  $\rho_i$ , and  $\rho_d$  are written in italics the number of counted tracks. Densities are expressed in  $10^6$  t/cm<sup>2</sup>. MTL = mean track length. Values in bracket for central age and MTL are, respectively, the number of single-grain ages and the number of lengths measured.  $1\sigma$  is the standard deviation. Dpar corresponds to a kinetic factor determined for each sample [Barbarand et al., 2003]. Neph. syen.: nephelinitic syenite.

useful as it can monitor different closure temperatures (as fission track length repartition) and is used to better constrain the thermal history (Figures 4 and S2). In addition, apatite grain chemistry impacts the damage-annealing rate and the AHe ages [Gautheron et al., 2013], as well as the broken crystal shapes [Brown et al., 2013]. The influence of chemistry has also been examined in this study, considering the Dpar range within each sample measured for AFT.

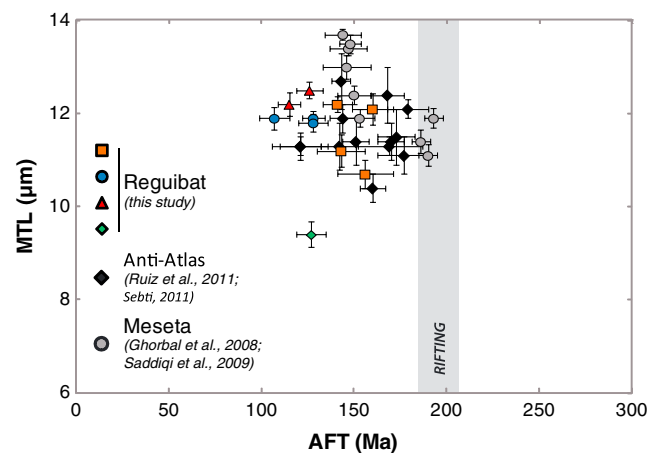


Figure 3. Mean track length (MTL) versus apatite fission track (AFT) ages plot, with standard deviation. We included all existing fission track data for the western Reguibat Shield (this study, same legend as Figure 1), the western Anti-Atlas [Ruiz et al., 2011; Sebt, 2011], and the Moroccan Meseta [Ghorbal et al., 2008; Saddiqi et al., 2009]. All data group within 100–200 Ma and 10–13  $\mu$ m, suggesting a potential similar postrift history for the whole margin.

Despite similar AFT and AHe data (Tables 1 and 2 and Figure 2) and geographical proximity (Figures 1b and 2), we grouped the individual samples of the Aousserd area to make two groups, AOS and SC. It is explained by the lithological differences between SC and AOS samples and the different AHe age-eU correlations (Figures 3 and S2). In the following thermal models, we use these two “grouped” samples instead of the individual ones for the samples from the northern Aousserd area.

### 3.3. Thermal Modeling

For our purposes, we used two modeling software tools: HeFTy [Ketcham, 2005] and QTQt [Gallagher, 2012]. We used QTQt software for the main modeling process. QTQt works with a probabilistic Bayesian approach for inverse modeling. It samples numerous thermal histories

**Table 2.** AHe Results<sup>a</sup>

Name	Crystal Dimensions ( $\mu\text{m}$ ) H-W-L <sup>b</sup>	Rs ( $\mu\text{m}$ )	Weight ( $\mu\text{g}$ )	$F_T$	4He (ncc/g)	U (ppm)	Th (ppm)	Sm (ppm)	Th/U	eU (ppm)	Age (Ma)	Age Corrected (Ma) <sup>c</sup>
AOS3A	188-113-100	57.7	4.14	0.78	379,656	30	40	403	1.4	43	74	95 ± 8
AOS3B	113-100-100	48.3	2.56	0.78	368,565	30	48	167	1.6	42	72	92 ± 7
AOS3C	188-113-100	58.4	5.02	0.80	168,336	28	29	318	1	37	38	47 ± 4
AOS3E	138-113-108	55	3.82	0.80	317,447	50	32	391	0.6	61	43	54 ± 4
AOS5A	88-138-138	54.4	3.77	0.84	176,56	9	8	125	0.8	12	12	14 ± 1
AOS5D	188-88-88	48.7	2.80	0.74	59,630	18	16	263	0.9	24	21	29 ± 2
AOS5F	125-100-113	48.2	2.27	0.75	175,595	29	24	195	0.8	37	39	52 ± 4
AOS2A	200-113-100	58.6	4.48	0.78	252,824	31	12	400	0.4	37	56	72 ± 6
AOS2B	213-113-131	62.7	6.65	0.81	219,641	23	16	105	0.7	28	65	81 ± 6
AOS2C	113-100-88	47	2.35	0.78	471,98	15	12	152	0.8	19	21	27 ± 2
AOS2D	113-88-88	43.8	1.96	0.76	77,464	20	31	179	1.5	29	22	29 ± 2
TCH7A	100-106-125	49.4	2.8	0.80	194,361	59	35	179	0.6	69	23	29 ± 2
TCH7B	213-138-113	68.7	8.03	0.83	137,470	19	23	339	1.2	28	41	50 ± 4
TCH7C	188-125-113	63.6	6.25	0.82	318,644	43	11	229	0.3	48	55	67 ± 5
TCH7D	150-131-150	64.6	6.31	0.84	106,664	13	9	267	0.7	18	50	59 ± 5
SC5A	150-88-88	46.9	2.61	0.76	209,790	21	5	83	0.3	23	77	101 ± 8
SC5C	163-113-100	56.6	4.35	0.80	26,664	6	6	16	1	8	28	35 ± 3
SC5D	213-113-100	59.9	5.69	0.80	214,047	27	11	15	0.4	30	60	75 ± 6
SC9B	188-113-113	59.9	5.40	0.81	59,285	7	12	271	1.7	12	42	52 ± 4
SC9D	150-75-75	41.4	1.92	0.72	282,683	27	37	274	1.4	38	62	86 ± 7
SC9E	125-88-100	45.8	2.35	0.76	606,341	52	66	401	1.3	71	71	93 ± 7
SC11C	138-100-94	50.3	3.01	0.78	18,224	5	4	284	0.9	8	19	24 ± 2
SC11D	181-138-125	68	7.34	0.84	92,904	7	14	228	1.8	12	62	74 ± 6
SC11E	138-113-113	53.2	2.98	0.78	157,370	11	25	103	2.2	18	71	92 ± 7
SC11F	188-138-125	66.7	5.97	0.82	47,093	8	3	266	0.4	11	35	43 ± 3
SC12A	100-85-85	41.6	1.65	0.75	108,424	10	13	232	1.4	15	61	82 ± 7
SC12D	175-125-125	64	6.22	0.83	180,770	19	9	241	0.5	23	64	78 ± 6
SC12G	138-100-100	49.5	2.44	0.75	222,395	22	13	141	0.6	26	48	63 ± 5
SC12F	138-113-100	52.3	2.80	0.77	151,382	25	26	360	1	34	55	71 ± 6
SC15A	125-138-113	59.7	4.73	0.83	141,644	11	16	382	1.5	18	67	80 ± 6
SC15B	163-113-113	56.5	3.70	0.78	16,791	4	9	126	2.4	7	21	27 ± 2
SC15F	138-100-88	48.3	2.27	0.75	50,901	6	20	90	3.5	11	39	52 ± 4
SC15G	113-131-113	56.5	3.99	0.83	234,089	25	24	340	0.9	34	57	69 ± 6
TAS233B	88-138-113	52.5	3.31	0.83	87,654	9	3	13	0.3	10	74	89 ± 7
TAS233F	150-113-100	55.5	4.01	0.80	163,092	36	13	9	0.4	39	35	43 ± 3
TAS233H	125-100-88	49.3	1.40	0.69	263,063	27	7	31	0.3	29	75	111 ± 9
TAS233D	138-125-113	58.8	4.58	0.82	55,323	6	2	14	0.3	7	65	79 ± 6
TAS233G	125-100-100	49.7	2.85	0.79	127,885	13	3	12	0.3	14	77	98 ± 8
TAS29A	188-138-125	5.97	5.97	0.82	168,828	14	5	12	0.4	15	90	111 ± 9
TAS29B	88-138-150	2	2.00	0.77	238,976	16	17	28	1.1	20	98	127 ± 10
TAS29C	138-100-113	2.57	2.57	0.76	196,140	20	5	10	0.3	21	78	102 ± 8
TAS29D	163-125-138	3.14	3.14	0.75	196,541	11	4	13	0.4	12	138	185 ± 15
TAS29E	163-188-138	7.22	7.22	0.84	57,789	7	2	7	0.3	8	62	74 ± 6

<sup>a</sup>Rs (sphere equivalent radius) and  $F_T$  (ejection factor) have been calculated using the developed procedure of *Gautheron and Tassan-Got* [2010] and *Ketchum et al.* [2011].

<sup>b</sup>Crystal dimensions. *H*: height of the prism; *W* and *L*: width and length, respectively, for the base of the prism. The width crosses the prism from two opposite angles and the length crosses the prism from two opposite faces. *L* and *W* are perpendicular.

<sup>c</sup>(U-Th-Sm)/He age corrected from alpha-ejection with the  $F_T$ .

and among them builds a population of models selected according to the degree of agreement between data and model—this is the burn-in phase. It then proceeds with inverse modeling, which is called the post burn-in phase. For each phase, the user can choose the number of iterations, depending on the complexity of its own data set. QTQt takes into account the more recent annealing model for fission tracks in apatite [*Ketchum et al.*, 2007], the two radiation damages annealing models of *Gautheron et al.* [2009] and *Flowers et al.* [2009], and incorporates a chemical proxy, either the Dpar or the chlorine content. Also, QTQt cannot take into account the individual crystal chemical variations and only handles a mean chemical value for all replicates. In QTQt, the fit between the data and the model is defined by the Log Likelihood (details are given in *Gallagher* [2012]), which gives a global value to estimate the fit of predicted data against the observed ones: the

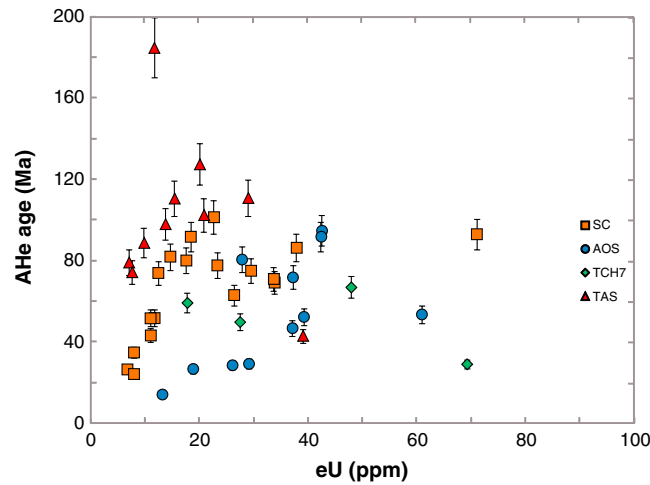


**Figure 4.** Plot of AHe ages versus eU (effective uranium content). Each sample group shows a rough correlation: the more the eU increases, the more the spread grows. Legends for different samples are the same as in Figure 1.

higher the Log Likelihood value, the better the solution is. Besides, the likelihood of a solution must be carefully checked through the stability of the solution.

The HeFTy software (which only uses the *Flowers et al.* [2009] He kinetics) and a homemade diffusion code program [Gautheron and Tassan-Got, 2010] (for the *Gautheron et al.* [2009] kinetics) were also used to monitor the apatites chemistry and size influence (see section 3.4 and Figures 5d, 6d, and 7d) through forward modeling. Both HeFTy software and our homemade diffusion code program can take into account not only the size of the apatite but also the chemistry through the use of  $r_{mr0}$  [Ketcham et al., 2007].

### 3.4. Strategy for Thermal Modeling

A three-step modeling procedure has been carried out using inverse and forward modeling with QTQt software [Gallagher, 2012]. This procedure is detailed in the supporting data.

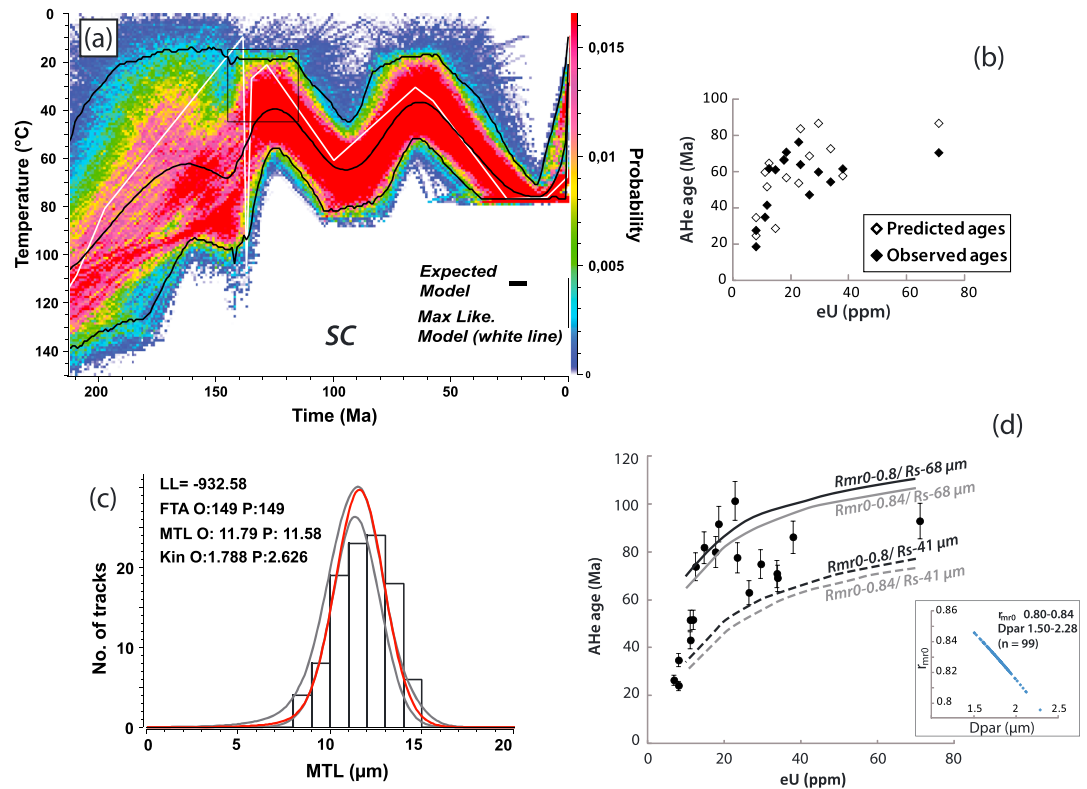


**Figure 5.** Final modeling for SC sample. It was processed through the *Gautheron et al.* [2009] code for the radiation damage and annealing. (a) Thermal history. Black box indicates the stratigraphical constraint of the Early Cretaceous. Max. Like: Maximum Likelihood model. (b) Predicted AHe ages against observed AHe ages. (c) Predicted lengths distribution (grey and red curves), mean track length (MTL) and Dpar (Kin) against the observed ones. FTA: Fission Track Age; O: Observed; P: Predicted; LL: Log Likelihood. (d) Predicted AHe-eU relationships for the thermal history of the expected model (black line in Figure 5a) given the  $r_{mr0}$  and the grain size ranges.

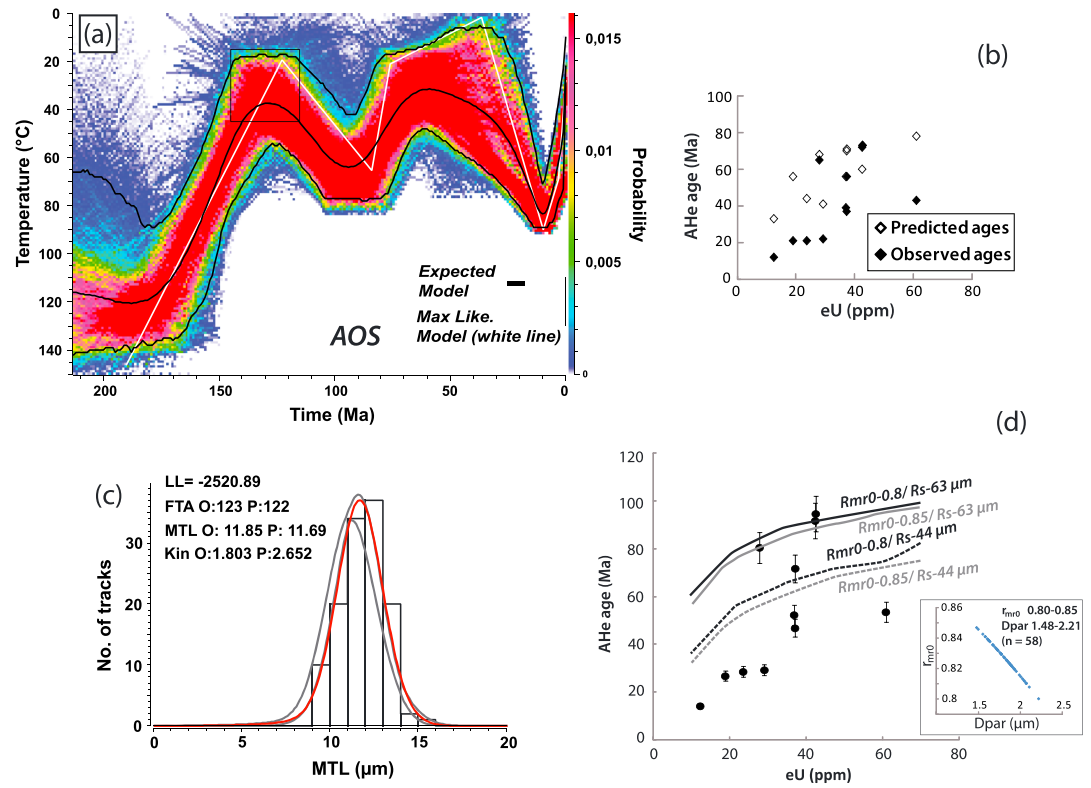


Figure 6. Final modeling for AOS sample. Legend is the same as Figure 5.

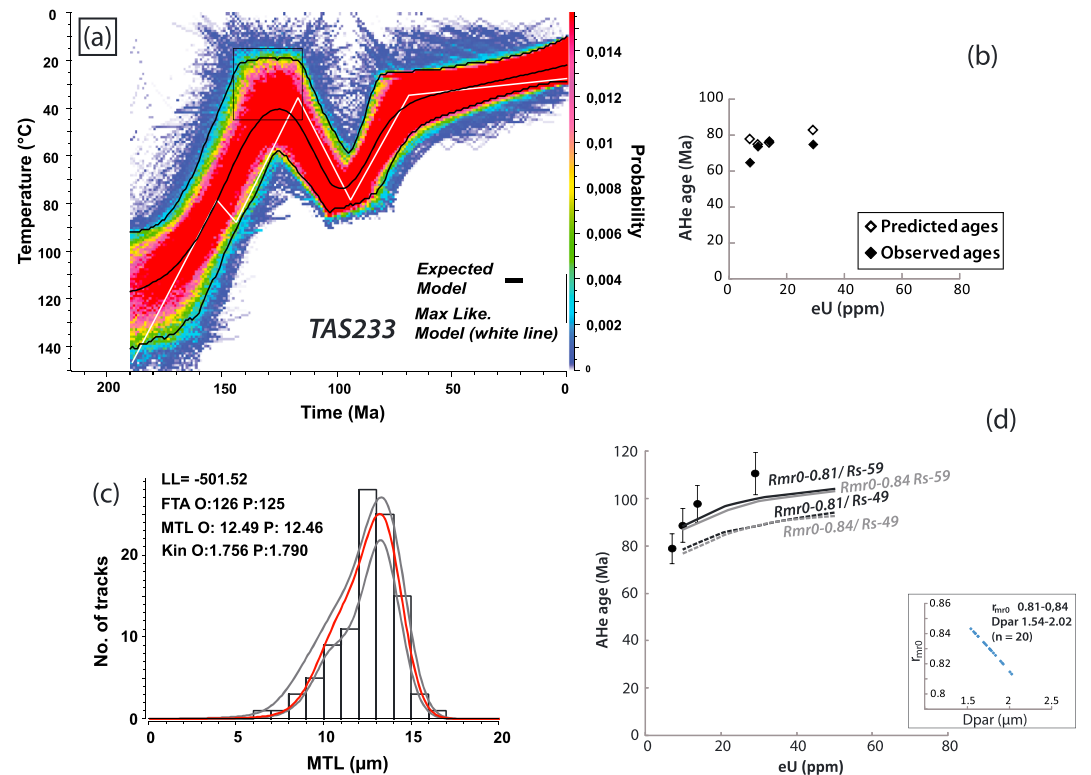


Figure 7. Final modeling for TAS233 sample. Legend is the same as Figure 5.

First, an exploratory inverse modeling was carried out in order to explore the (T,t) space and search for likely common thermal histories between samples (Figure S3, Tables S1–S3, and Text S1). The QTQt software was run without (T,t) constraints but was unable to yield stable solutions. Consequently, we used two conditions to narrow the (T,t) space to explore the following: (1) a stratigraphical constraint given by Lower Cretaceous units lying unconformably on the Reguibat basement less than 100 km from the samples (Figure 1a; see *Wissmann* [1982] for the southern area), indicating that they were close to or at the surface at that time, and (2) a data-dependent result, i.e., the fact that AFT ages are bracketed between 107 and 175 Ma plus their length distributions and Mean Track Lengths (MTLs), implying that samples must have been at temperatures higher than 110°C before 200 Ma (Figure S4). Otherwise we would expect more scattered and older AFT ages and different track length distributions. Considering these two facts, we ran inverse modelings, which were also not able to give very stable solutions (Figures S5 and S6).

Second, representative thermal histories obtained through this first modeling step were tested through forward modeling so as to refine and restrain the possible thermal paths (Figure S7, Text S2, and Tables S4 and S5). The resultant selected thermal paths indicate the best probable thermal paths.

Lastly, final inverse modelings, incorporating the results of the previous tests, were run to investigate the degrees of freedom left to the model for a better fit to the data (Figures 5–7 and S8–S10). For each sample, we present in Figures 5–7 the final thermal modelings resulting from the use of the *Gautheron et al.* [2009] kinetics. Nevertheless, both radiation damage and annealing models were run and gave comparable results (see Figures S8–S10 for final modelings with the *Flowers et al.* [2009] kinetics).

In addition to these modelings, forward modeling with HeFTy and a homemade diffusion code (for the *Gautheron et al.* [2009] kinetics) were used in order to explain the scatter in AHe data. Given the final obtained thermal histories (Figures 5a, 6a, and 7a), we processed these in forward modeling, varying the grain size and the chemistry to assess their primary roles on the dispersion (Figures 5d, 6d, and 7d).

## 4. Results

### 4.1. Thermochronometry

AFT ages range from  $107 \pm 8$  to  $175 \pm 16$  Ma, with mean track length ranging from  $11.8 \pm 0.19 \mu\text{m}$  to  $12.5 \pm 0.18 \mu\text{m}$  (Table 1). Overall, AFT ages are quite homogenous, around 130–140 Ma (Figures 2 and 3). Mean track lengths (MTLs) are quite uniformly distributed within the studied region (Figures 2 and 3). The distribution of lengths shows a mean centered on  $12 \mu\text{m}$ , with a significant standard deviation of  $\sim 1.8 \mu\text{m}$  (Figure S1). The difference between AFT ages and crystallization ages shows that these were reset ( $T > 110^\circ\text{C}$ ) and underwent significant time residence in the partial annealing zone (60–110°C). One peculiar observation is that all our AFT ages are younger than the rifting (Figure 3). This does not preclude the existence of an exhumation at the time of the rifting but implies younger steps of cooling whose amplitude would have bleached this first exhumation phase.

AHe ages corrected from the alpha-ejection range from  $14 \pm 1$  Ma to  $185 \pm 15$  Ma (Table 2). AHe ages show a large scatter from significantly younger to comparable ages than the AFT ones (Figure 2). eU contents also display a wide range from 7 to 71 ppm. For the AOS and SC samples (Figure 1b), very young AHe ages (younger or close to  $\sim 20$  Ma) record a final pulse of recent cooling. AHe ages have been plotted against eU content for each group of samples (Figures 4 and S2). A positive correlation exists when samples are grouped regionally (SC and AOS in the north; TAS samples in the south; Figures 1b, 3, and S2). The AHe replicates of one single sample, TCH7, do not exhibit a clear correlation, and their AHe ages are no younger than  $\sim 29$  Ma. Overall, the southern TAS samples show AHe age ranges that are older than northern AOS and SC samples (74–127 Ma against 24–101 Ma, respectively).

### 4.2. Final Inverse Modelings

After the modeling procedure described in section 3.4, Figures 5–7 summarize the main results of the modeling for three sample groups (SC and AOS grouped samples and TAS233, which is similar to TAS29; Table 2). For all samples, we ran QTQt with 10,000 iterations for the burn-in phase. Given the complexity of AOS and SC data sets, 150,000 iterations were run for the post burn-in phase, whereas only 100,000 iterations were run for TAS233 sample, which is less complex.

Two types of thermal history appear from modeling. The southern group (TAS233; Figures 7a and S10) shows a polyphased history with two cooling events, whereas northern groups show the same events plus a third recent cooling event (Figures 5a, 6a, S8, and S9). Overall, the same cooling trends (1) from 200 Ma to the Early Cretaceous (60–80°C in 70 Ma) and (2) from the base of the Late Cretaceous (~95 Ma) to the early Paleogene (30–40°C in 35 Ma), can be observed in all thermal paths, with very similar magnitudes and cooling rate. After this, two different types of thermal histories are recorded, with a slow cooling for the southern region (from 40 to 20°C during the Cenozoic) and a renewed burial followed by recent denudation for the northern region (exhumation from the Miocene at 70–80°C to the present at ~20°C). This last event explains the larger dispersion of AHe ages for the samples of the northern area, compared to the southern one, since they show corrected AHe ages younger than 70 Ma (Table 2).

The comparison between predicted and measured data shows Log Likelihood values ranging between –2520 and –501 (Log Likelihood (LL) in Figures 5c, 6c, 7c, and S8–S10). The stability of the solutions has been assessed, and only modelings with the more stable solutions are presented here (Figure S11). Very negative values of Log Likelihood have been found when AHe age replicates were the most scattered (for AOS and SC samples), whereas they prove to be fairly good for the TAS233 sample. This scatter in AOS and SC data sets also generates instabilities in the solutions (Figure S11).

### 4.3. Dispersion Within LT Thermochronology Data Sets

Given the final thermal histories of each sample (Figures 5a, 6a, 7a, and S8–S10) and knowing the range of eU, we can then determine the theoretical expected AHe age variations [Flowers *et al.*, 2009; Gautheron *et al.*, 2009]. This has been done in Figures 5d, 6d, and 7d, considering the size range and the chemistry variability of the apatites (Table 2). The range of Dpar values of the AFT samples (Table 1) was used as the proxy for estimating the variation of chemistries within each sample and incorporated into the AHe age predictions of Figures 5d, 6d, and 7d (converted into  $r_{mro}$ , according to Ketcham *et al.* [2007]). The mean thermal histories obtained with the final inverse modelings were then treated in forward modeling, varying the  $r_{mro}$  and the range size. The mean thermal histories obtained through the use of the Gautheron *et al.* [2009] kinetics were processed with a homemade diffusion code program [Gautheron and Tassan-Got, 2010] (Figures 5d, 6d, and 7d). The same is presented for the Flowers *et al.* [2009] kinetics using the HeFTy software (Figures S8–S10) with comparable results.

Except for a few points in each sample and a less good reproduction for the AOS sample, taking into account both the chemistry and the apatite size enables us to reproduce the scatter range for the AOS and SC samples (Figures 5d, 6d, 7d, and S8–S10). The combination of both parameters shows ranges of dispersion of between a few degrees to more than 30°C. The “simpler” thermal history of the TAS233 sample together with restricted chemistry variations makes the dispersion of its AHe ages comparatively less than for the two others (Figures 7d and S10). Also, we used the mean thermal histories (Figures S8–S10) to estimate the closure temperature according to the formulation of Flowers *et al.* [2009] given a range of eU values (Figure S12). It shows that samples from the northern area have a 55–120°C closure temperature range, whereas those from the southern area display a more limited 55–85°C range, related to the simpler thermal history.

## 5. Discussion

### 5.1. Postrift Evolution of the South Moroccan Margin

#### 5.1.1. Late Jurassic and Early Cretaceous Cooling

All thermal histories are characterized by a cooling signal recorded from the Early to Late Jurassic until mid-Early Cretaceous (Figures 5a, 6a, and 7a), from temperatures higher than 110°C (at ~200 Ma) to 30–40°C in ~70 Ma. These temperatures higher than 110°C before 200 Ma may be explained by either the presence of basement or sedimentary rocks on top of the now outcropping rocks or a higher heat flow, or both.

A major heat pulse must have occurred at the Triassic–Jurassic boundary, with the setting of the Central Atlantic Magmatic Province (CAMP) [Marzoli *et al.*, 1999; Verati *et al.*, 2005]. This magmatic province extended over Northeast America, the WAC, and the northeast of South America. Brown *et al.* [1994] studied the influence of the Karoo volcanism on the thermal record of the Karoo basin. They showed an important thermal impact of the volcanism for the first 5 km of the upper crust, in the case of significant thicknesses of intrusive and/or extrusive igneous rocks. Until now, no igneous rocks from the CAMP have been discovered on the Reguibat

Shield basement and a thick basaltic layer covering the northern craton at that time is unlikely. The CAMP is thus thought to have poorly influenced the thermal record showed by our thermal history at the sample locations. Furthermore, samples are located quite far from the stretched crust (more than 150 km; Figure 2). In the case of the margin behaving like the northern section in the Meseta (see Figure 9 for location) [Maillard *et al.*, 2006], i.e., with a simple shear model, the African plate being the upper one, existing thermomechanical models predict significant thermal heat flow anomalies in a very narrow zone restricted to the stretched crust [Voorhoeve and Houseman, 1988; Issler *et al.*, 1989]. Finally, given their location at more than 150 km from the hinge line, is it unlikely for our samples to have undergone significant heating effects of both the CAMP event and the thermal effects linked to the rifting between 200 and 190 Ma.

The South Moroccan passive margin then recorded a minimum 70–80°C cooling after our modeling results, which suggests that denudation is the main cause of the recorded cooling at that time. No estimates of the paleogeotherm for the Moroccan passive margin have been published. Nevertheless, from *Sehrt* [2014], we can derive rough estimates of this paleogeotherm for the southern Anti-Atlas (location in Figure 9). For the Early Cretaceous, the mean paleogeotherm is  $48 \pm 25^\circ\text{C km}^{-1}$ , whereas it seems to decrease afterward, to  $40 \pm 28^\circ\text{C km}^{-1}$  in the Late Cretaceous until present values around  $30\text{--}35^\circ\text{C km}^{-1}$ . Given a rough range of 30 to  $50^\circ\text{C km}^{-1}$  for the paleogeotherm, we can derive denudation rates of  $12\text{--}29 \text{ m Ma}^{-1}$  and total denudation minimum estimates from 0.8 to 2 km (with a 70°C cooling during 70 Ma).

As already suggested by *Leprêtre et al.* [2013] for the central Reguibat Shield, the basement could have been buried under a significant but now eroded Paleozoic cover (~1–2 km). It does not exclude a contribution from the Proterozoic basement in the western Reguibat Shield. Two huge deltas developed in the TLDB during the Early Cretaceous, at the latitude of TanTan and Boujdour [AUXINI, 1969; Mitchum and Vail, 1977; Ranke *et al.*, 1982; Abou Ali *et al.*, 2004]. They show a prograding trend bypassing the edge of the Jurassic paleoshelf, with a typical forced regression prism in the TanTan delta [Mitchum and Vail, 1977]. This trend is confirmed at the latitude of Dakhla, by the seismic profiles of *Labails et al.* [2009], where a bypass also occurred. The importance of the denudation is demonstrated by (1) the abundant material feeding immense prograding deltaic systems [AUXINI, 1969; Ranke *et al.*, 1982] and (2) the nature of this material, which mainly comes from the Paleozoic cover [Martinis and Visintin, 1966] and the cratonic basement [Einsele and von Rad, 1979; Ali *et al.*, 2014] (Figure 8a). All these observations, plus the detrital/coarse nature of the sediments, are well explained by the amplitude and duration of the cooling trend that affects the margin.

The infill of the TLDB at that time could also be partly sourced in the Anti-Atlas as suggested by the existing LT thermochronology results [Ruiz *et al.*, 2011; Sebt, 2011]. A recent provenance study in the northern TLDB negatively concludes on this issue [Ali *et al.*, 2014], whereas field observations in the Lower Cretaceous formations in the northern TLDB show the deposition of Anti-Atlas materials [Martinis and Visintin, 1966; E. C. Rjimat, personal communication, 2013].

### 5.1.2. Mid-Early Cretaceous to Late Cretaceous Reheating

After the surface conditions of the Early Cretaceous, our thermal histories record a 30–40°C reheating from the Aptian to the Turonian, within 30–40 Ma (Figures 5–7). There is no evidence at that time of any important magmatic event that could account for this reheating [Guiraud *et al.*, 2005]. We thus interpret the cooling that happened to be the result of a kilometer-scale burial generated by an active subsidence from the end of the Neocomian to the Cenomanian-Turonian times. This active subsidence occurred at quite low rates of  $\sim 15\text{--}43 \text{ m Ma}^{-1}$  (for  $30\text{--}50^\circ\text{C km}^{-1}$  end-members geotherms, a 30–40°C total cooling and 30–40 Ma duration of the cooling).

In Aptian-Albian times, an important transgression took place [Martinis and Visintin, 1966], followed by the Cenomanian-Turonian maximum sea level high stand [Miller *et al.*, 2005]. In this peculiar context, the active subsidence led to the deposition of shallow marine carbonates during Aptian-Albian times that can reach a kilometer thick cover [Martinis and Visintin, 1966; AUXINI, 1969]. Then, the TLDB underwent extensive shallow marine carbonate to deep-marine sediments deposition during Cenomanian-Coniacian times in its northern part [Ranke *et al.*, 1982]. This cover is eroded, south of 24°N (Figure 1b). Average thickness where it has not been eroded can reach 200–300 m between Laayoune and Boujdour [AUXINI, 1969; Ranke *et al.*, 1982]. The original thickness might be thicker since the top of the formation often shows an erosional unconformity with the overlying detrital early Paleogene [von Rad and Wissmann, 1982]. Our results prove that this Aptian to Turonian cover should have also existed landward (Figure 8b).

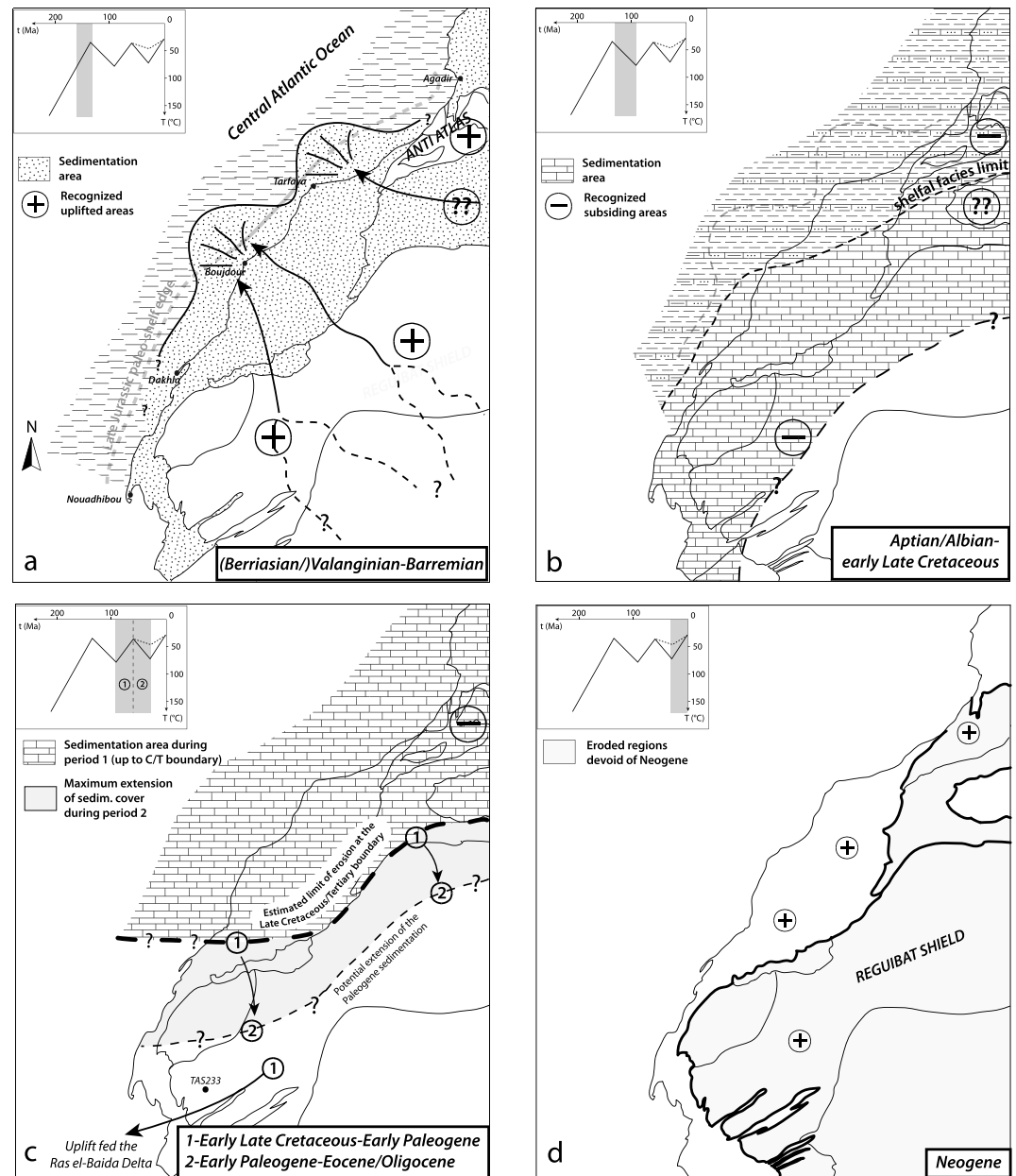


**Figure 8.** Schematic evolution of the South Moroccan Passive Margin during Mesozoic-Cenozoic times, based on our thermochronology results and published data on the western Anti-Atlas [Ghorbal *et al.*, 2008; Saddiqi *et al.*, 2009; Ruiz *et al.*, 2011; Sebti, 2011]. For each step, the expected model for the thermal history of the northern samples (SC and AOS) is presented in solid black line, and for Tertiary times, we added the expected model of the southern samples (TAS) with a dotted black line. (a) Berriasian-Valanginian evolution. (b) Aptian/Albian to early Late Cretaceous evolution. (c) Two steps of time: 1 = early Late Cretaceous to early Paleogene and 2 = early Paleogene to Eocene/Oligocene transition. (d) Neogene evolution.

### 5.1.3. Cooling at the Beginning of the Late Cretaceous

The observed  $\sim 30^{\circ}\text{C}$  cooling during the Late Cretaceous had lasted for 30–35 Ma (Figures 5–7). With two end-member paleogeotherms ranging between 30 and  $50^{\circ}\text{C km}^{-1}$ , we expect denudation rates ranging from 20 to  $40\text{ m Ma}^{-1}$ . Since we have no record of the Late Cretaceous in the onshore southern TLDB, we cannot directly correlate what happens inland with the offshore record. Our theory is that the majority of the Early Cretaceous sequence plus some early Late Cretaceous formations has been removed from the Reguibat Shield basement.

West Africa witnessed important geodynamic events during the mid-Cretaceous transition. Mainly based on Atlantic magnetic isochrones, the kinematic study of *Rosenbaum et al.* [2002] showed that the onset of the convergence between Africa and Europe occurred between 120 and 83 Ma. Opening of the South Atlantic Ocean occurs during Aptian-Albian times [*Moulin et al.*, 2010] and continues afterward northward. This opening is responsible for the propagation of intracontinental rifts from the apex of the South Atlantic in the Gulf of Guinea landward, which followed the Pan-African suture east of the WAC [*Guiraud and Maurin*, 1992]. At the same time, the anticlockwise rotation of Northeast Africa led to the following: (1) episodes of rifting south of the Hoggar [*Bosworth*, 1992; *Browne and Fairhead*, 1983] and (2) compression north of it. These northern compressive events are known as the Austrian phase [*Boudjema*, 1987] and set north/south (N/S) structures, parallel to the N/S fault zones of the Pan-African suture.

The deformations linked to the Austrian events are closely localized around the Pan-African suture [*Boudjema*, 1987], and it is unlikely that they left imprints on the margin, so far from the major structures. The cooling we have identified likely results from geodynamic reorganization, i.e., the Africa-Europe convergence that could transmit stress across the plate leading to long-wavelength deformation. This hypothesis has been formulated by *Frizon de Lamotte et al.* [2009] based on the observation that Cenomanian-Turonian deposits are lacking on both the Reguibat Shield and the Anti-Atlas. The authors advocated that large approximately ENE/WSW lithosphere anticlines could have developed during the post-Turonian/ante-Oligocene period, removing the cover. It can be also seen in the Tindouf Basin, where Cenomanian-Turonian formations are truncated and unconformably overlain by Paleogene sediments [*Fabre*, 2005]. Nonetheless, no cooling event has yet been detected in the western Anti-Atlas, and early Late Cretaceous times show a differentiation between the western Reguibat Shield and the western Anti-Atlas (Figure 8c).

This cooling phase, not recognized until now, is also compatible with the development of important deltas south of the Reguibat Shield, as the offshore Mauritania witnessed the formation of the Ras al-Beida delta [*Davison*, 2005] (Figure 8c). It would imply that the drainage network had been reworked at that time compared to the Neocomian (Figure 8a), driving the sediments southward due to the different regional slope.

#### 5.1.4. Late Cretaceous-Tertiary Stage

A common thermal path exists from the Late Cretaceous to the Cretaceous-Tertiary boundary for the western Reguibat Shield (Figures 5–7). Nevertheless, whereas the western Reguibat Shield is cooling until the Cretaceous-Paleogene transition, the western Anti-Atlas was kept buried until middle/late Paleogene times, below a kilometer thick sedimentary cover [*Ruiz et al.*, 2011; *Sebti*, 2011] (Figures 9d and 9e). This period shows the development of a spatial differentiation in the pattern of exhumation along the passive margin from the western Anti-Atlas to the western Reguibat Shield, separating a domain north of the TLDB from a domain south of it.

For Tertiary onward, focusing on the western Reguibat shield, we see that the northern groups are in a reheating phase until Miocene times (Figures 5 and 6), whereas the southern group shows a quite stable thermal state, or a slow cooling, until the present day (Figure 7). We think that this north/south difference lies within the limited extension of a Paleogene cover over the Reguibat shield. Outliers of Paleogene survived onto the western Reguibat Shield basement [*Ratschiller*, 1968] but do not exist southward (Figure 1b), suggesting that the cover may have never reached this area or has been recently eroded and/or was thinner (Figure 8d). The result is that a progressive differentiation occurred from the beginning of the Tertiary in the western part of the Reguibat shield, between the north, bounding the TLDB and the south, north of the Senegal basin. If we compare our thermal histories to the western Anti-Atlas data (Figures 5–7 and 9), both regions exhumed from important temperatures (60–80°C) from Eocene to Early Miocene times (Figure 8d). Contrary to the western Anti-Atlas, whose exhumation is often related to a thermal component [*Teixell et al.*, 2005; *Missenard et al.*, 2006], the exhumation of the western Reguibat Shield is more enigmatic at that time.

This final and puzzling cooling pulse, in the western Reguibat Shield, is recorded by the northern groups during the Neogene, whereas no significant temperature peak is modeled for by the southern group for the same period (Figures 5–7). During the Neogene occurred the final convergence steps in the Atlas orogen. Moreover, this period corresponds to an icehouse age from the Oligocene onward. We think that both hypotheses represent potential causes to explain the variation between the northern groups and the southern one. The convergence could initiate lithospheric folds similar to the early Late Cretaceous period,

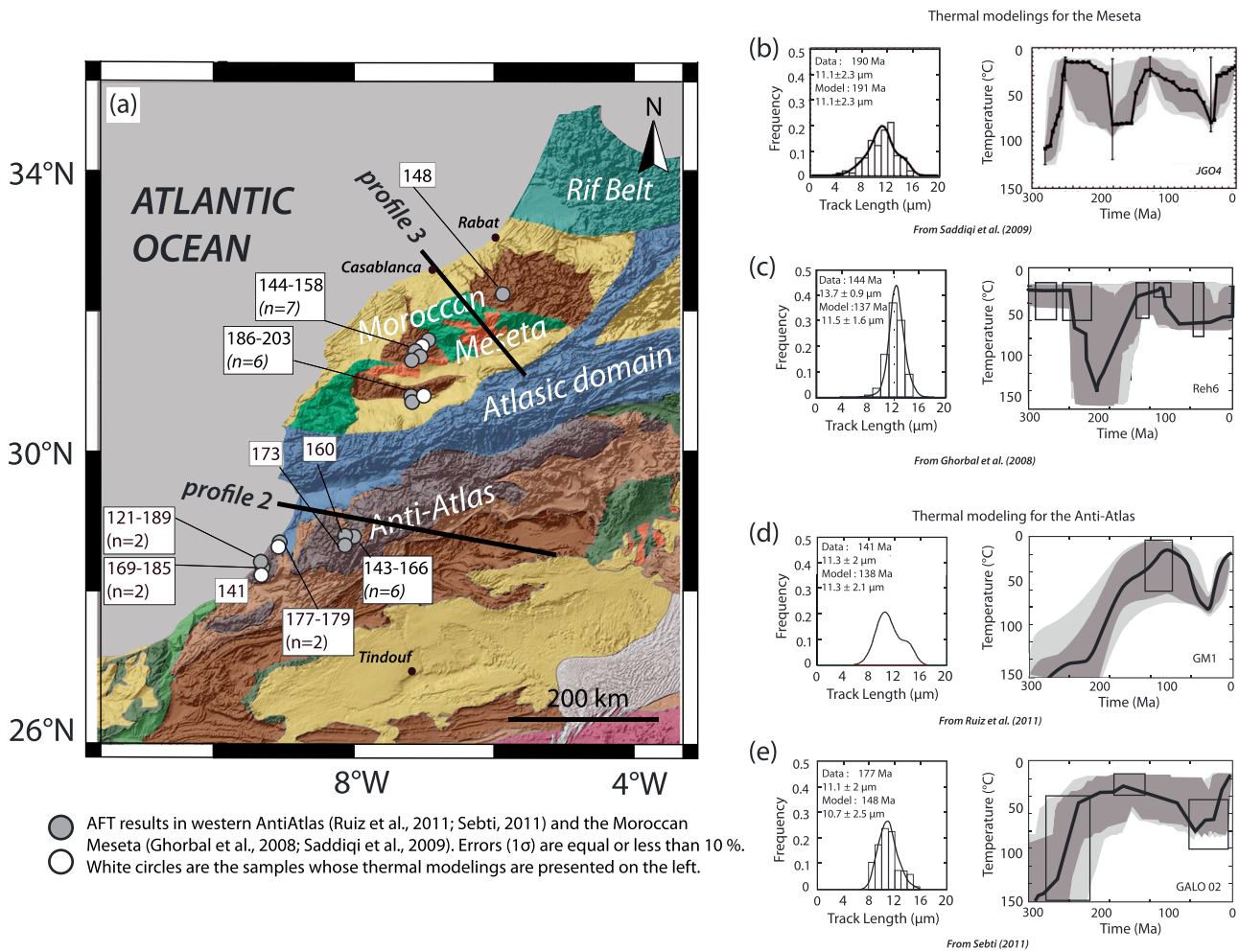


**Figure 9.** Summary of the LT thermochronology published results (AFT ages) for the northern part of the passive margin of Morocco. (a) General geological map of northern Morocco. AFT ages are given in the white boxes, with  $n$  indicating the number of samples when they are more than one. Circles locate the sample of the various studies. Errors ( $1\sigma$ ) on AFT ages are within 10%. Used colors are the same as in Figure 1b, except for the Rif and the Atlasic belts (green and blue, respectively). Profiles 2 and 3 are also localized in Figure 1a in a wider geographical scale, together with profile 1. (b–e) Thermal modelings from the LT thermochronology studies of Saddiqi et al. [2009], Ghorbal et al. [2008], Ruiz et al. [2011], and Sebti [2011], respectively. For the modelings of Ghorbal et al. [2008] (sample Reh6) and Ruiz et al. [2011] (sample GM1), we led a forward modeling with their obtained thermal path, to deduce the modeled parameters (lengths and modeled AFT age). We present the HeFTy modelings provided within these previous works, as we did not have access to the whole data sets to make new modelings with QTQt software.

creating regional differential uplift. Nonetheless, there is no evidence such as unconformities or tectonic structures that can be linked to a putative folding event. Climatic forcing could provide another explanation, but we must consider that northern and southern groups belong to different drainage basins. In this scenario, the high-frequency sea level variations actively erode the margin close to the shore (samples from northern area SC and AOS), whereas the southern samples TAS would belong to a landward drainage basin, less affected by erosion. Given the proximity of the latter to the shoreline, this second hypothesis is unlikely, and we favor the hypothesis of a large scale folding of the lithosphere.

### 5.2. The Low-Elevated Character of the Moroccan Passive Margin

Here we will discuss the occurrence of the cooling/heating events revealed by our modeling and how we relate them to the shaping of the low-lying Northwest African margin. Its evolution is then considered in comparison to its northeast American counterpart.

#### 5.2.1. Early Postrift Evolution: Jurassic to Early Cretaceous

Predictions of the morphological shaping of passive margins after breakup have been made for high-elevated passive margins using AFT results [Gallagher et al., 1998]. The plotting of AFT ages of the western Reguibat

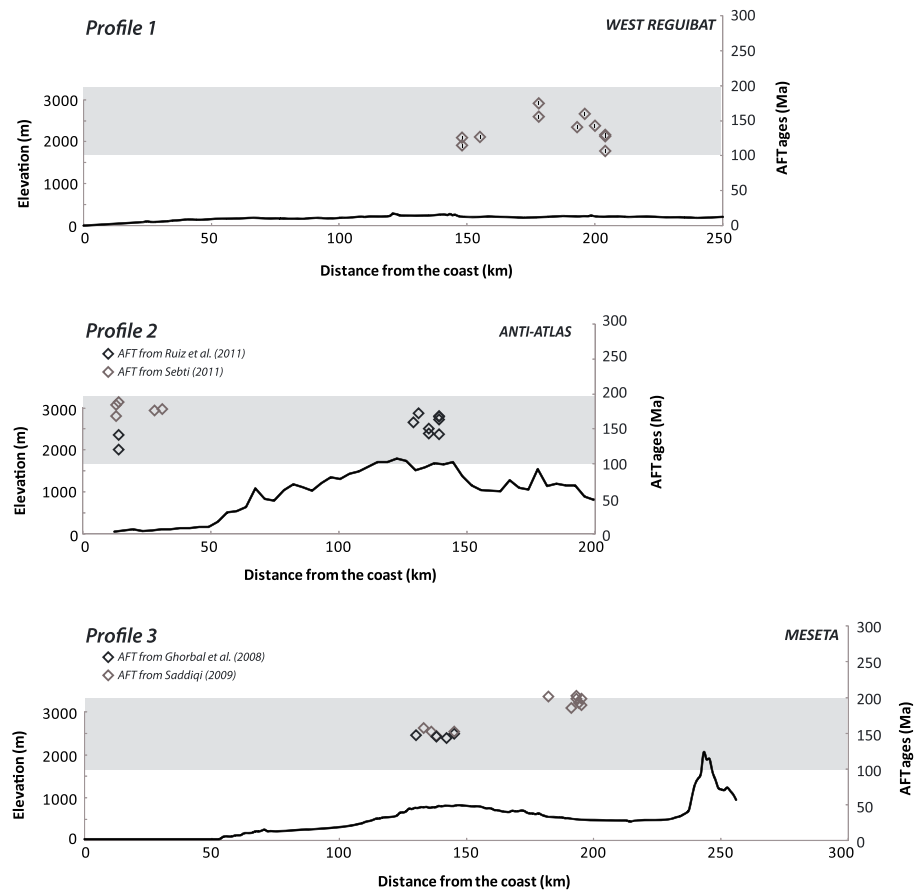


**Figure 10.** AFT ages against the distance from the hinge line, for the western Reguibat Shield (profile 1), the western Anti-Atlas (profile 2), and the Moroccan Meseta (profile 3), plotted above elevation profiles of each geographical setting. Elevation profiles are located in Figure 1a. AFT ages come from *Ghorbal et al.* [2008] and *Saddiqi et al.* [2009] for the Moroccan Meseta and *Ruiz et al.* [2011] and *Sebti* [2011] for the western Anti-Atlas and from this study. The hinge line is used as defined in *Labails et al.* [2009] and is fixed at distance = 0 km on each plot. Grey domains encompass the whole observed variation in  $F_T$  ages for the three geological settings. Whatever the geological setting and the distance inland, the AFT ages are bracketed within the same age range (100–200 Ma) and do not show any dependency to the margin setting.

Shield (this study), the western Anti-Atlas [*Ruiz et al.*, 2011; *Sebti*, 2011] and the Meseta [*Ghorbal et al.*, 2008; *Saddiqi et al.*, 2009] against the distance from the hinge line could then give reliable information about the mechanisms of the early postrift (Figure 10). Although AFT ages along the margin span between 100 and 200 Ma, it is not possible to demonstrate any correlation with the distance to the hinge line (Figure 10). Indeed, the “boomerang plot” of *Gallagher and Brown* [1997] plots spanning up to ~250 km inland is not visible here (Figure 3). This boomerang plot represents a typical feature of many high-elevated passive margins that show a coastal plain separated from a high-elevated plateau by a steep sea-facing escarpment (up to 1–2 km in height). The absence of the boomerang plot means either (1) that this preexisting topography was eroded during postrift or (2) that this kind of topography never existed. The first hypothesis would imply progressive erosion of the landward high plateau, and we would expect a younging trend for AFT ages landward becoming potentially younger than the rifting, which is not the case. Instead, the second hypothesis considers a more uniform and “constant” topography that did not differentiate enough to be recorded through AFT and AHe methodology. Here AFT ages are equal to or younger than the rifting ages (Figure 3). This “young” signal expresses the strong protracted large-scale denudation event still going on in the early postrift times (up to 60–70 Ma after the breakup). This event does not rule out the possibility of an early structuring following the classic scheme of a flanked rift. Nevertheless, in this case, it would have been a weak relief and this situation would have been quickly disrupted by the protracted denudation event that affected the whole width of the margin, as far as 200–250 km inland.

**Table 3.** Estimations of Erosion Rates During the Late Jurassic/Early Cretaceous Cooling Event Derived From AFT Studies on the Meseta and the Anti-Atlas<sup>a</sup>

Samples	Time lapse (Ma)	Temperature Variation (°C)	Cooling Rate (°C Ma <sup>-1</sup> )	Erosion Rates, Given a Paleogeotherm (m/Ma)	
				30°C km <sup>-1</sup>	50°C km <sup>-1</sup>
<i>Ghorbal et al. [2008]</i>					
Reh5	40	90	2.25	75	45
Reh6	60	110	1.8	60	36
Reh9	40	100	2.5	83	50
Zae	20	70	3.5	117	70
<i>Saddiqi et al. [2009]</i>					
JTB2	30	50	1.7	57	34
RH9a	50	75	1.5	50	30
JGO4	50	55	1.1	37	22
RH8	30	60	2	67	40
<i>Ruiz et al. [2011]</i>					
GM1	60	100	1.7	57	34
GDI3-3	75	60	0.8	27	16
TAF3	90	60	0.7	23	14
TAF6	95	130	1.4	47	28
TAF22	55	80	1.5	50	30

<sup>a</sup>Two end-member paleogeotherms have been considered for each region (30°C km<sup>-1</sup> and 50°C km<sup>-1</sup>). The time lapse is the estimated time of this specific cooling event for each thermal modelings. The temperature variation is the calculated decrease of temperature during the cooling event.

Denudation rates of Middle to Late Jurassic/Early Cretaceous cooling along the margin are presented in Table 3, for the three margin sections (with AFT data of *Ghorbal et al. [2008]*, *Saddiqi et al. [2009]*, *Ruiz et al. [2011]*, *Sebti [2011]* and this study). We chose two realistic end-members for the paleogeotherm values (see section 5.1.1), spreading from 30 to 50°C km<sup>-1</sup>. The mean minimum denudation rates, for the 50°C km<sup>-1</sup> paleogeotherm, range from (1) 22 to 70 m Ma<sup>-1</sup> for the Meseta, (2) 14 to 34 m Ma<sup>-1</sup> for the western Anti-Atlas, and (3) 12 to 29 m Ma<sup>-1</sup> for the western Reguibat Shield (and are multiplied by 5/3 for 30°C km<sup>-1</sup>). These rates share the same order of magnitude. Besides, the Meseta seems to have undergone a stronger denudation that could tentatively be explained by its crossroads location, being the rift flank of both the central Atlantic Ocean to the west and the Tethys to the east. Overall, this convergence of denudation rate values across the more than 2000 km of the Moroccan passive margin points to a unique event affecting it, within the same amplitude range for the whole length of the margin. We propose that this large-scale denudation event is related to the central Atlantic evolution but unconnected to the rifting phases.

### 5.2.2. Early Postrift Evolution: Aptian to Turonian

Our results show that active subsidence produced the kilometric-scale burial after the Neocomian until Cenomanian-Turonian times. The same scheme applies for the evolution of the Anti-Atlas and the Meseta in the north, where thermal modeling shows a similar heating trend after the mid-Early Cretaceous events (Figures 5–7) and is symptomatic of the burial of the Anti-Atlas and the Meseta at that time [*Ghorbal et al., 2008*; *Saddiqi et al., 2009*; *Sebti, 2011*; *Ruiz et al., 2011*] (Figure 9). Overall, all the subsiding basements of the margin from the South Moroccan section to the Anti-Atlas section and in the north into the passive margin of the Meseta show the same amplitude of ~30–50°C reheating (Figure 9). The peculiarity of the whole margin is that it is also extensively covered by marine Cenomanian-Turonian deposits whose extension can reach several hundred kilometers landward [*Gevin, unpublished, 1974*; *Choubert et al., 1966*; *Martinis and Visintin, 1966*; *Haddoumi et al., 2008*; *Zouhri et al., 2008*]. It is also constantly showing marine deposits under shallow environments without important lateral thickness variations. Such an extension with a constant marine character requires the paleosurface at that time to have been considerably flattened. It means that no significant differential topographical anomaly existed before and rules out the possibility of a surviving high topography landward on the passive margin after 100 Ma since the initiation of the first major detrital input in the Early Cretaceous.

Remarkably, within the northwestern WAC the Reguibat Shield reveals a very poor preservation of the Cenomanian-Turonian deposits and it might have been either a relatively higher topographical zone compared to the rest of the area or the subsequent cooling event during the Late Cretaceous may have wiped out a thinner Aptian-Turonian cover.

Our modeling and the synthesis of the LT thermochronology results along the whole passive margin show that this kilometeric burial after Neocomian times is an active one. It cannot be explained by the transgression phase initiated during the Aptian-Albian alone, which has a far weaker amplitude (estimated to +100/200 m [Miller *et al.*, 2005]). We postulate that the greater the burial was, the greater the transgression appeared and seems to have been overlooked in the case of the Moroccan passive margin.

### 5.2.3. Early Postrift Evolution and Mechanisms

The Early Cretaceous “event,” i.e., the setting of the huge deltaic systems at that time is still unsolved (see discussion in von Rad and Sarti [1986]). We have shown that the onset of these deltaic systems is associated with a general denudation episode for the whole Moroccan margin. Tectonic hypothesis to explain this long-lasting cooling must be rejected: no compressive features can be found at that time in this region and no compressional settings existed either [Choubert *et al.*, 1966; El Khatib, 1995; Le Roy, 1997; Davison, 2005; Guiraud *et al.*, 2005]. A compressive context might have begun to interfere only during the Early/Late Cretaceous transition [Rosenbaum *et al.*, 2002].

To explain the stratigraphical structure and subsidence curves of the northern TLDB, Gouiza [2011] has proposed the hypothesis of a thermal anomaly, linked to a late stage of rifting associated with lithospheric necking during the Early Jurassic (200–190 Ma), but the study restricted itself to the narrow marginal thinned domain. This hypothesis explains the subsequent abnormally high subsidence of the offshore margin during the Late Jurassic and the Early Cretaceous combined with the onshore exhumation of the basement of the Reguibat Shield by isostatic response. Nevertheless, it fails to reproduce the posterior reheating phase in the end of the Early Cretaceous, which is observed along the whole margin on the onshore basements of the Meseta, the western Anti-Atlas, and the western Reguibat Shield.

We propose two hypotheses to account for the homogeneity of AFT ages along the 200 km width of the margin. First, a thermally supported uplift such as lithospheric thinning either by delamination (e.g., for the North China Craton in Deng *et al.* [2007]) or thermal erosion (e.g., by the impact of a plume, see Olson *et al.* [1988]) could be responsible for this uplift and denudation event affecting the whole passive margin (e.g., Figure 8a). Second, a dynamically supported uplift is also plausible with rapid lithospheric mantle motions due to either the lateral density difference between the two lithospheres [Huismans and Beaumont, 2011] or the geometry of the continent-ocean lithospheric boundary [Armitage *et al.*, 2013]. For example, Armitage *et al.* [2013] used numerical modeling of the small convection cells at the interface oceanic/continental lithosphere to show their ability to generate dynamic topography at 200 km or more landward. These two hypotheses are more satisfying than a mechanical hypothesis alone (like flexural effects) as they could explain that a significant continental strip of the margin exhumed as a whole, instead of following the more usual scheme linked to the distance to the ocean. However, the lithospheric thinning hypothesis is unlikely. In the case of the delamination, it is a dramatic event that can last ~10 Ma or less [Bird, 1979]. We have interpreted the Late Jurassic/Early Cretaceous cooling event as a denudation one (section 5.1.1) and given its duration (~50 Ma or more) a delamination would barely explain the long-lasting cooling trend we observe during the Late Jurassic/Early Cretaceous (Figures 5a, 6a, and 7a). In the case of thermal erosion, the problem of the reconstruction of the thermal root of the lithosphere is similar to what happens after delamination. Bird [1979] showed that the duration of this reconstruction of the root, associated with a decrease of the topography is significantly longer than the 30 Ma of reheating that occurred from Aptian to Turonian. Moreover, lithospheric thinning is a process, which is often accompanied by magmatic effects that we cannot see here. We then favored the dynamically supported uplift scenario since it has the advantage of explaining the renewed and active subsidence from Aptian to Turonian: an active subsidence will subsequently follow when the convection cells break down. Besides, we suggest that the active subsidence could have also been enhanced by the load represented by the Lower Cretaceous deposits on the margin crust.

### 5.3. Comparison With the Northeast American Passive Margin

There is no remnant of an escarpment on the Moroccan passive margin (Figure 2) and our interpretation suggests that no high-elevated plateau has ever been formed. On the contrary, based on LT thermochronology and basin drainage analysis, Spotila *et al.* [2004] concluded that the Blue Ridge Escarpment, on the conjugate American margin, located as far as 400 km from the present margin in the southern Appalachian, is the remnant of an escarpment whose evolution goes back to the central Atlantic

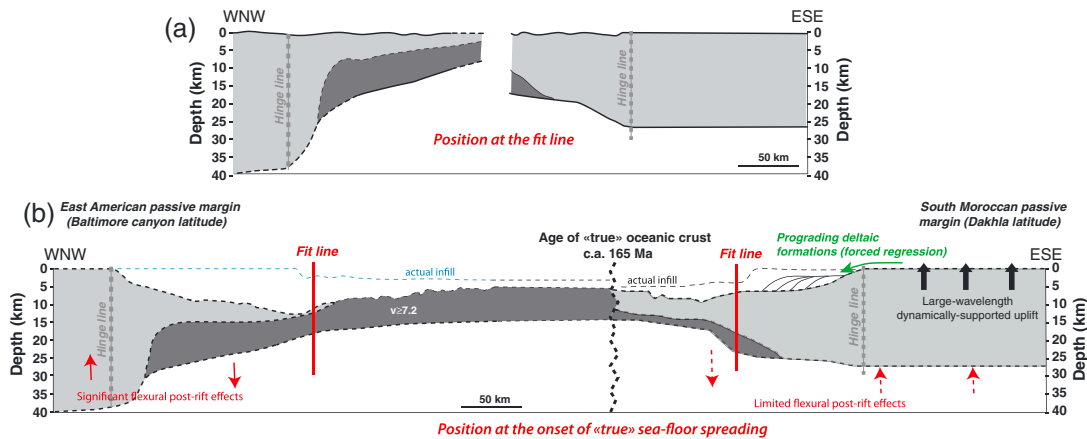


**Figure 11.** (a) Comparison of passive margins crusts cross sections from Northeast America and South Morocco (modified after *Labails et al.* [2009]). The stretched African margin is slightly narrower than the American one, at crustal and maybe lithospheric scale. (b) Reconstruction at the onset of seafloor spreading (modified after *Labails et al.* [2009]). We show the prograding character of Lower Cretaceous detrital deposits on the TLDB offshore basin and the actual infills in both margin basins in thin dotted lines. Red arrows show the importance of the flexural effects for each margin (weak for the African one and strong for the American one; see discussion in section 5.3). Dark bold arrows show the widely distributed exhumation during the Early Cretaceous on the African continental margin.

rifting. High elevations on passive margins, often assumed to be surviving relics of an old topography are now generally considered to result from flexural effects [*Weissel and Karner, 1989; van der Beek et al., 1994*].

The crustal structure of the Moroccan passive margin at the western Anti-Atlas latitude is not well known at the continent-ocean transition, but the Anti-Atlas and the Reguibat Shield both belong to the WAC [*Ennih and Liégeois, 2008*], and they probably share a similar deep crustal shape. *Labails et al.* [2009] show that the continental domain at the latitude of Dakhla suffered limited extension during the rifting of the central Atlantic Ocean, leaving a very narrowly thinned crustal domain. Due to their common inherited history, it is likely that the thinning of the continental lithosphere at the western Anti-Atlas latitude is also rather narrow (approximately 100 km; Figures 11a and 11b). Moreover, this could also be the case for the whole northwest passive margin of Africa, since this is also demonstrated by seismic analysis on the passive margin of the Moroccan Meseta [*Maillard et al., 2006*].

The difference between the ~100 km and ~180 km of stretching for the African margin [*Maillard et al., 2006; Labails et al., 2009*], and its American counterpart (see Figure 11b) [*Miall et al., 2008*] should be the first important feature that controls the setting of a topography. *Van der Beek et al.* [1994], using thermomechanical models, showed that the greater the stretching, the less the potential topography will be. In the African-American conjugate system, the stretching difference is not really significant, but the narrower African stretched crust should produce more topography on this side. In flexural models, one important aspect is the required asymmetry between the stretching of the crust versus the lithosphere and their lateral offset to be able to produce high topography [*Weissel and Karner, 1989; van der Beek et al., 1994*]. This aspect is hard to discuss in our case, since the only reconstruction is the one of *Maillard et al.* [2006] for the Moroccan Meseta and the Canadian conjugate margin and does not easily allow conclusions to be drawn. One last important parameter is the elastic thickness of each plate and how the plates retained strength during the rifting, i.e., how the competition between the thinning of the crust and the heat flow are affecting its strength [*Watts, 2012*].

With respect to all these parameters, based on Figure 11, we can state that the stretching length is not significantly different for the two margins and the crustal thinning is similar, though seemingly higher for the American crust. Besides, initial rheology might have favored more rigidity for the Moroccan margin, more cratonized [*Ennih and Liégeois, 2008*], compared to the American margin, which represents a volcanic margin [*Grant, 1977; Austin et al., 1990; Sheridan et al., 1993*], likely to have undergone greater heat flow disruption that would have reduced its strength [*Watts, 2012*]. Lastly, the offshore stratigraphy points out a quite symmetrical development from rifting until the Early Cretaceous [*Jansa and Wiedman, 1982*]. Paradoxically, the two conjugate margins appear quite symmetrical, except as regards their initial rheology and the unknown stretching factors of the crust versus the lithosphere. The stronger African margin might have behaved more rigidly compared to the weaker American one, impeding the development of an important

topography. The support of the American topography, in this case could be explained by both the weaker strength of its lithosphere and the potential variation in the stretching factors acting on a crustal and lithospheric scale [Weissel and Karner, 1989; van der Beek et al., 1994] compared to the African margin.

This conclusion, mainly drawn upon facts related to the rifting itself, seems to stress the importance of the early stages in the development of the topographical identity of the passive margins. It tends to favor the idea that the variable existing topographies on actual passive margins are primarily controlled by the rifting stages instead of being features acquired in the course of their postrift evolution.

## 6. Conclusion

We have led the first integrated thermochronological study for the South Moroccan passive margin in order to propose its first integrated geological history. The combined use of AFT and AHe methodology with the stratigraphical record has been essential and allows us to show a complex postrift history:

1. A common major Late Jurassic/Early Cretaceous cooling, affecting the whole passive margin. This event cannot be solely linked to the rifting. For now, we suggest that mantle dynamics can account for the fact that the entire width of the margin underwent kilometer-scale denudation.
2. A common active subsidence phase occurred from Aptian to Turonian. This event affected the whole Northwest African margin and allowed the deposition of Cenomanian-Turonian shallow marine deposits far inland. This remarkable fact forces us to consider that by 100 Ma, the topography was highly flattened on the whole passive margin.
3. A cooling event in the Late Cretaceous that we link to the onset of the Africa/Europe convergence.
4. A slow cooling for the southern samples of the western Reguibat Shield during Paleogene and reheating for northern samples at the same time, followed by a rapid cooling from Miocene onward. Tertiary histories for the Meseta and the western Anti-Atlas are fundamentally different since they have exhumed since the end of the Paleocene. The evolution of the northern section of the Moroccan margin reflects the geodynamic changes due to the Atlas formation.

Our thermal modeling results allow us to account for the stratigraphical record primarily in the basin (offshore/onshore) and confirm the need to look for an available record of the onshore burial/exhumation trends to give a reliable reconstruction of the sedimentary realm evolution.

We have demonstrated that the Northwest African margin, along more than 2000 km from the Meseta to the western Reguibat Shield shares a similar early postrift history from the breakup at ~190 Ma to Cenomanian-Turonian. Such a common history of the whole passive margin indicates, first, not only the importance of its lithospheric structure and the geometry of breakup but also the overprint of a very wide scale dynamically supported uplift event that resulted in a large-scale flattening of the pre-Late Cretaceous surface.

Together with other similar studies along Atlantic coasts, our work aims for a renewal in the study of low-elevated passive margins. This study points out the very poor knowledge we have on their evolution compared to the high-elevated ones, although it is clear that they have undergone complex postrift histories with kilometeric-scale vertical motions. Finally, our study stresses that in the case of the African and American conjugate margins the topographical identity of each margin seems to be acquired during the early stages of their development and might not be due to late postrift features.

## Acknowledgments

We thank Eric Douville for accessing the ICP-MS (LSCE, Gif-sur-Yvette) and Louise Bordier for the U-Th measurements. The quality of English language has been greatly improved thanks to Andrew Arnoll. This work has been supported by the Académie Hassan II des Sciences and Techniques, Rabat, Morocco. R. Leprêtre is a recipient of a PhD fellowship from the Ecole Normale Supérieure (ENS), Paris.

## References

- Abou Ali, N., E. H. Chellaïe, and M. Nahim (2004), Anatomie d'une marge passive hybride. Marge Ifni/Tan-Tan (sud du Maroc) au Mésozoïque: Apports des données géophysiques, *Estud. Geol.*, 60(3–6), 111–121, doi:10.3989/egeol.04603-683.
- Ali, S., K. Stattegger, D. Garbe-Schönberg, W. Kuhnt, O. Kluth, and H. Jabour (2014), Petrography and geochemistry of Cretaceous to quaternary siliciclastic rocks in the Tarfaya basin, SW Morocco: Implications for tectonic setting, weathering, and provenance, *Int. J. Earth Sci.*, 103, 265–280, doi:10.1007/s00531-013-0965-6.
- Armitage, J. J., C. Jaupart, L. Fourrel, and P. A. Allen (2013), The instability of continental passive margins and its effect on continental topography and heat flow, *J. Geophys. Res. Solid Earth*, 118, 1817–1836, doi:10.1002/jgrb.50097.
- Austin, J. A., P. L. Stoffa, J. D. Philipps, J. Oh, D. S. Sawyer, G. Michael Purdy, E. Reiter, and J. Makris (1990), Crustal structure of the Southeast Georgia embayment-Carolina trough: Preliminary results of a composite seismic image of a continental suture (?) and a volcanic passive margin, *Geology*, 18(10), 1023–1027, doi:10.1130/0091-7613(1990)018.
- AUXINI (1969), Correlacion estratigrafica de los sondeos perforados en el Sahara Español, *Bol. Geol. Minero*, 83, 235–251.
- Barbarand, J., A. Carter, I. Wood, and T. Hurford (2003), Compositional and structural control of fission-track annealing in apatite, *Chem. Geol.*, 198, 107–137, doi:10.1016/S0009-2541(02)00424-2.

- Bea, F., P. Montero, F. Haissen, and A. El Archi (2013), 2.46 Ga kalsilite and nepheline syenites from the Awsard pluton, Reguibat Rise of the West African Craton, Morocco. Generation of extremely K-rich magmas at the Archean–Proterozoic transition, *Precambrian Res.*, *224*, 242–254, doi:10.1016/j.precamres.2012.09.024.
- Beauvais, A., and D. Chardon (2013), Modes, tempo, and spatial variability of Cenozoic cratonic denudation: The West African example, *Geochem. Geophys. Geosyst.*, *14*, 1590–1608, doi:10.1002/ggge.20093.
- Bird, P. (1979), Continental delamination and the Colorado Plateau, *J. Geophys. Res.*, *84*(B13), 7561–7571, doi:10.1029/JB084iB13p07561.
- Bishop, P. (2007), Long-term landscape evolution: Linking tectonics and surface processes, *Earth Surf. Proc. Landforms*, *32*, 329–365, doi:10.1002/esp.1493.
- Bonow, J. M., P. Japsen, and T. F. D. Nielsen (2014), High-level landscapes along the margin of southern East Greenland—A record of tectonic uplift and incision after breakup in the NE Atlantic, *Global Planet. Change*, *116*, 10–29, doi:10.1016/j.gloplacha.2014.01.010.
- Bosworth, W. (1992), Mesozoic and early Tertiary rift tectonics in East Africa, *Tectonophysics*, *209*, 115–137, doi:10.1016/0040-1951(92)90014-W.
- Boudjema, A. (1987), Evolution structurale du bassin pétrolier “triasique” du Sahara nord oriental (Algérie), PhD thesis, Univ. Paris-sud, France.
- Brown, R. W., K. Gallagher, and M. Duane (1994), A quantitative assessment of the effects of magmatism on the thermal history of the Karoo sedimentary sequence, *J. Afr. Earth Sci.*, *18*(3), 227–243, doi:10.1016/0899-5362(94)90007-8.
- Brown, R. W., M. A. Summerfield, and A. J. W. Gleadow (2002), Denudational history along a transect across the Drakensberg Escarpment of southern Africa derived from apatite fission track thermochronology, *J. Geophys. Res.*, *107*(B12), 2350, doi:10.1029/2001JB000745.
- Brown, R. W., R. Beucher, S. Roper, C. Persano, F. Stuart, and P. Fitzgerald (2013), Natural age dispersion arising from the analysis of broken crystals: Part I. Theoretical basis and implications for the apatite (U–Th)/He thermochronometer, *Geochim. Cosmochim. Acta*, *122*, 478–497, doi:10.1016/j.gca.2013.05.041.
- Brown, R. W., M. Summerfield, A. Gleadow, K. Gallagher, A. Carter, R. Beucher, and M. Wildman (2014), Intracontinental deformation in southern Africa during the Late Cretaceous, *J. Afr. Earth Sci.*, *100*, 20–41, doi:10.1016/j.jafrearsci.2014.05.014.
- Browne, S. E., and J. D. Fairhead (1983), Gravity study of the Central African Rift System: A model of continental disruption: 1. The Ngaoundere and Abu Gabra Rifts, *Tectonophysics*, *94*, 187–203, doi:10.1016/0040-1951(83)90016-1.
- Chardon, D. (1997), Les déformations continentales archéennes. Exemples naturels et modélisation thermomécanique, PhD thesis, Univ. de Rennes I, France.
- Choubert, G., A. Faure-Muret, and L. Hottinger (1966), *Aperçu Géologique du Bassin Côtier de Tarfaya, Notes et Mém. du Service Géol.*, vol. 175, pp. 218, Editions du Service Géologique du Maroc, Rabat, Maroc.
- Cogné, N., K. Gallagher, P. R. Cobbold, C. Riccomini, and C. Gautheron (2012), Post-breakup tectonics in southeast Brazil from thermochronological data and combined inverse-forward thermal history modeling, *J. Geophys. Res.*, *117*, B11413, doi:10.1029/2012JB009340.
- Davison, I. (2005), Central Atlantic margin basins of North West Africa: Geology and hydrocarbon potential (Morocco to Guinea), *J. Afr. Earth Sci.*, *43*, 254–274, doi:10.1016/j.jafrearsci.2005.07.018.
- Deng, J., S. Su, Y. Niu, C. Liu, G. Zhao, X. Zhao, S. Zhou, and Z. Wu (2007), A possible model for the lithospheric thinning of North China Craton: Evidence from the Yanshanian (Jura–Cretaceous) magmatism and tectonism, *Lithos*, *96*, 22–35, doi:10.1016/j.lithos.2006.09.009.
- Dodson, M. H. (1973), Closure temperature in cooling geochronological and petrological systems, *Contrib. Mineral. Petrol.*, *40*, 259–274.
- Einsele, G., and U. von Rad (1979), Facies and paleoenvironment of Early Cretaceous sediments in DSDP site 397 and in the Aaiun Basin (NW Africa), in *Initial Reports Deep Sea Drilling Project*, vol. 47, edited by U. von Rad et al., pp. 559–577, U.S. Govt Printing Office, Washington, D. C.
- El Khatib, J. (1995), Etude structural et stratigraphique d’un segment de la marge continentale atlantique sud-marocaine: Le bassin de Tarfaya-Laâyoune, PhD thesis, Univ. de Nice-Sophia Antipolis, France.
- Ennih, N., and J. P. Liégeois (2008), The boundaries of the West African Craton, with special reference to the basement of the Moroccan metacratonic Anti-Atlas belt, in *The Boundaries of the West African Craton, Geol. Soc. Spec. Publ.*, vol. 297, edited by N. Ennih, and J. P. Liégeois, pp. 1–17, Geol. Soc. London, doi:10.1144/SP297.1.
- Fabre, J. (2005), *Géologie du Sahara Occidental et Central, Tervuren African Geoscience Collection*, vol. 108, Musée Royal de l’Afrique Central, Belgium.
- Flowers, R., R. A. Ketcham, D. Shuster, and K. A. Farley (2009), Apatite (U–Th)/He thermochronology using a radiation damage accumulation and annealing model, *Geochim. Cosmochim. Acta*, *73*, 2347–2365, doi:10.1016/j.gca.2009.01.015.
- Frizon de Lamotte, D., P. Leturmy, Y. Missenard, S. Khomsi, G. Ruiz, O. Saddiqi, F. Guillocheau, and A. Michard (2009), Mesozoic and Cenozoic vertical movements in the Atlas system (Algeria, Morocco, Tunisia): An overview, *Tectonophysics*, *475*, 9–28, doi:10.1016/j.tecto.2008.10.024.
- Galbraith, R. F., and G. M. Laslett (1993), Statistical models for mixed fission track ages, *Nucl. Tracks Radiat. Meas.*, *21*, 459–480, doi:10.1016/1359-0189(93)90185-C.
- Gallagher, K. (2012), Transdimensional inverse thermal history modeling for quantitative thermochronology, *J. Geophys. Res.*, *117*, B02408, doi:10.1029/2011JB008825.
- Gallagher, K., and R. W. Brown (1997), The onshore record of passive margin evolution, *J. Geol. Soc. London*, *154*, 451–457, doi:10.1144/gsjgs.154.3.0451.
- Gallagher, K., R. W. Brown, and C. Johnson (1998), Fission track analysis and its applications to geological problems, *Annu. Rev. Earth Planet. Sci.*, *26*(5), 9–72, doi:10.1146/annurev.earth.26.1.519.
- Gautheron, C., and L. Tassan-Got (2010), A Monte Carlo approach to diffusion applied to noble gas/helium thermochronology, *Chem. Geol.*, *273*(3–4), 212–224, doi:10.1016/j.chemgeo.2010.02.023.
- Gautheron, C., L. Tassan-got, J. Barbarand, and M. Pagel (2009), Effect of alpha-damage annealing on apatite (U–Th)/He thermochronology, *Chem. Geol.*, *266*, 166–179, doi:10.1016/j.chemgeo.2009.06.001.
- Gautheron, C., J. Barbarand, R. A. Ketcham, L. Tassan-Got, P. van der Beek, M. Pagel, R. Pinna-Jamme, F. Couffignal, and M. Fialin (2013), Chemical influence on  $\alpha$ -recoil damage annealing in apatite: Implications for (U–Th)/He dating, *Chem. Geol.*, *351*, 257–267, doi:10.1016/j.chemgeo.2013.05.027.
- Ghorbal, B., G. Bertotti, J. Foeken, and P. Andriessen (2008), Unexpected Jurassic to Neogene vertical movements in “stable” parts of NW Africa revealed by low temperature geochronology, *Terra Nova*, *20*(5), 355–363, doi:10.1111/j.1365-3121.2008.00828.x.
- Gleadow, A. J. W., and I. R. Duddy (1981), A natural long-term track annealing experiment for apatite, *Nucl. Tracks*, *5*, 169–174, doi:10.1016/0191-278X(81)90039-1.
- Gouiza, M. (2011), Mesozoic source-to-sink systems in NW Africa: Geology of vertical movements during the birth and growth of the Moroccan rifted margin, PhD thesis, VU Univ. Amsterdam, Netherlands.
- Grant, A. C. (1977), Multichannel seismic reflection profiles of the continental crust beneath the Newfoundland Ridge, *Nature*, *270*(5632), 22–25, doi:10.1038/270022a0.
- Guiraud, R., and J. C. Maurin (1992), Early Cretaceous rifts of Western and Central Africa: An overview, in geodynamics of rifting: Vol. II. Case history studies on rifts: North and South America, Africa-Arabia, *Tectonophysics*, *213*(1–2), 153–168, doi:10.1016/0040-1951(92)90256-6.

- Guiraud, R., W. Bosworth, J. Thierry, and A. Delplanque (2005), Phanerozoic geological evolution of Northern and Central Africa: An overview, *J. Afr. Earth Sci.*, **43**, 83–143, doi:10.1016/j.jafrearsci.2005.07.017.
- Haddoumi, H., A. Charrière, B. Andreu, and P.-O. Mojon (2008), Les dépôts continentaux du Jurassique moyen au Crétacé inférieur dans le Haut-Atlas oriental (Maroc): Paléoenvironnements successifs et signification paléogéographique, in *Carnets de Géologie—Notebooks on Geology*, pp. 1765–2553, INIST-CNRS, Brest, 2008/XX (CG2008 AX). [Available at: <http://paleopolis.reidir.es/cg/>]
- Hafid, M., G. Tari, D. Bouhadioui, I. El Moussaid, H. Echarfaoui, A. Ait Salem, M. Nahim, and M. Dakki (2008), Atlantic basins, in *Continental Evolution: The Geology of Morocco, Lect. Notes Earth Sci.*, vol. 116, edited by A. Michard, et al., pp. 303–329, doi:10.1007/978-3-540-77076-3\_6.
- Harman, R., K. Gallagher, R. W. Brown, and A. Raza (1998), Accelerated denudation and tectonic/geomorphic reactivation of the cratons of northeastern Brazil during the Late Cretaceous, *J. Geophys. Res.*, **103**(B11), 27,091–27,105, doi:10.1029/98JB02524.
- Holford, S. P., P. F. Green, I. R. Duddy, J. P. Turner, R. R. Hillis, and M. S. Stoker (2009), Regional intraplate exhumation episodes related to plate-boundary deformation, *Geol. Soc. Am. Bull.*, **121**(11–12), 1611–1628, doi:10.1130/B26481.1.
- Huismans, R., and C. Beaumont (2011), Depth-dependent extension, two-stage breakup and cratonic underplating at rifted margins, *Nature*, **473**, 74–79, doi:10.1038/nature09988.
- Hurford, A. J. (1990), Standardization of fission track dating calibration: Recommendation by the Fission Track Working Group of the I.U.G.S. Subcommission on Geochronology, *Chem. Geol.*, **80**, 171–178, doi:10.1016/0168-9622(90)90025-8.
- Hurford, A. J., and P. F. Green (1983), The Zeta age Calibration of fission-track dating, *Isotope Geosci.*, **1**, 285–317, doi:10.1016/S0009-2541(83)80026-6.
- Issler, D., H. McQueen, and C. Beaumont (1989), Thermal and isostatic consequences of simple shear extension of the continental lithosphere, *Earth Planet. Sci. Lett.*, **91**, 341–358, doi:10.1007/978-3-540-77076-3\_6.
- Jansa, L. F., and J. Wiedman (1982), Mesozoic-Cenozoic development of the Eastern North American and Northwest African continental margins: A comparison, in *Geology of the Northwestern African Continental Margin*, edited by U. von Rad et al., pp. 215–269, Springer, New York, doi:10.1007/978-3-642-68409-8\_11.
- Japsen, P., J. A. Chalmers, P. F. Green, and J. M. Bonow (2012), Elevated, passive continental margins: Not rift shoulders, but expressions of episodic, post-rift burial and exhumation, *Global Planet. Change*, **90–91**, 73–86, doi:10.1016/j.gloplacha.2011.05.004.
- Japsen, P., P. F. Green, and J. A. Chalmers (2014), The mountains of North-East Greenland are not remnants of the Caledonian topography, *Tectonophysics*, **589**, 234–238, doi:10.1016/j.tecto.2012.07.026.
- Johnson, C., and K. Gallagher (2000), A preliminary Mesozoic and Cenozoic denudation history of the North East Greenland onshore margin, *Global Planet. Change*, **24**, 261–274, doi:10.1016/S0921-8181(00)00012-6.
- Ketcham, R. A. (2005), Forward and inverse modeling of low-temperature thermochronometry data, *Rev. Mineral. Geochem.*, **58**(1), 275–314, doi:10.2138/rmg.2005.58.11.
- Ketcham, R. A., A. Carter, R. A. Donelick, J. Barbarand, and A. J. Hurford (2007), Improved modeling of fission-track annealing in apatite, *Am. Mineral.*, **92**, 799–810, doi:10.2138/am.2007.2281.
- Ketcham, R. A., C. Gautheron, and L. Tassan-Got (2011), Accounting for long alpha-particle stopping distances in (U–Th–Sm)/He geochronology: Refinement of the baseline case, *Geochim. Cosmochim. Acta*, **75**(24), 7779–7791, doi:10.1016/j.gca.2011.10.011.
- Klingelhoefer, F., C. Labails, E. Cosquer, S. Rouzo, L. Géli, D. Aslanian, J. L. Olivet, M. Sahabi, H. Nouzé, and P. Unternehr (2009), Deep crustal structure of the SW Moroccan margin from wide-angle and reflection seismic data (The DAKHLA experiment), *Tectonophysics*, **468**, 63–82, doi:10.1016/j.tecto.2008.07.022.
- Kraml, M., R. Pik, M. Rahn, R. Selbekk, J. Carignan, and J. Keller (2006), A new multi-mineral age reference material for  $^{40}\text{Ar}/^{39}\text{Ar}$  (U–Th)/He and fission track dating methods: The Limberg t3 tuff, *Geostand. Geoanal. Res.*, **30**, 73–86, doi:10.1111/j.1751-908X.2006.tb00914.x.
- Labails, C., J. L. Olivet, and The Dakhla study group (2009), Crustal structure of the SW Moroccan margin from wide-angle and reflection seismic data (the Dakhla experiment). Part B—The tectonic heritage, *Tectonophysics*, **468**, 83–97, doi:10.1016/j.tecto.2008.08.028.
- Labails, C., J. L. Olivet, D. Aslanian, and W. R. Roest (2010), An alternative early opening scenario for the central Atlantic Ocean, *Earth Planet. Sci. Lett.*, **297**, 355–368, doi:10.1016/j.epsl.2010.06.024.
- Le Roy, P. (1997), Les Bassins Ouest-Marocains: Leur formation et leur evolution dans de cadre de l'ouverture et du developpement de l'Atlantique Central (Marge Africaine), PhD thesis, Univ. de Brest, France.
- Leprêtre, R., J. Barbarand, Y. Missenard, F. Leparmentier, and D. Frizon de Lamotte (2013), Vertical movements along the northern border of the West African Craton: The Reguibat Shield and adjacent basins, *Geol. Mag.*, doi:10.1017/S0016756813000939.
- Maillard, A., J. Malod, E. Thiébot, F. Klingelhoefer, and J. P. Réhault (2006), Imaging a lithospheric detachment at the continent-ocean crustal transition off Morocco, *Earth Planet. Sci. Lett.*, **241**, 686–698, doi:10.1016/j.epsl.2005.11.013.
- Martinis, B., and V. Visintin (1966), Données géologiques sur le bassin sédimentaire côtier de Tarfaya, in *Sedimentary Basins of the African Coasts: Part 1. Atlantic Coast*, edited by D. Reyre, pp. 13–26, Association des Services Géologiques Africains, Paris, France.
- Marzoli, A., P. R. Renne, E. M. Piccirillo, M. Ernesto, G. Bellien, and A. De Min (1999), Extensive 200-million-year-old continental flood basalts of the Central Atlantic Magmatic Province, *Science*, **284**, 616–618, doi:10.1126/science.284.5414.616.
- McDowell, F. W., W. C. McIntosh, and K. A. Farley (2005), A precise  $^{40}\text{Ar}$ – $^{39}\text{Ar}$  reference age for the Durango apatite (U–Th)/He and fission-track dating standard, *Chem. Geol.*, **214**(3–4), 249–263, doi:10.1016/j.chemgeo.2004.10.002.
- Miall, A. D., H. R. Balkwill, and J. McCracken (2008), The Atlantic margin basins of North America, in *The Sedimentary Basins of the United States and Canada, Sediment. Basins of the World*, vol. 5, edited by A. D. Miall, pp. 473–504, Elsevier, Amsterdam, Boston, Heidelberg, doi:10.1016/S1874-5997(08)00014-2.
- Michard, A., A. Soulaimani, C. Hoepffner, H. Ouanaïmi, L. Baïdier, E. C. Rjimati, and O. Saddiqi (2010), The South-Western branch of the Variscan Belt: Evidence from Morocco, *Tectonophysics*, **492**, 1–24, doi:10.1016/j.tecto.2010.05.021.
- Miller, K. G., M. A. Kominz, J. V. Browning, J. D. Wright, G. S. Mountain, M. E. Katz, P. J. Sugarman, B. S. Cramer, N. Christie-Blick, and S. F. Pekar (2005), The Phanerozoic record of global sea-level change, *Science*, **310**(5752), 1293–1298, doi:10.1126/science.1116412.
- Missenard, Y., H. Zeyen, D. Frizon de Lamotte, P. Leturmy, C. Petit, M. Sébrier, and O. Saddiqi (2006), Crustal versus asthenospheric origin of relief of the Atlas Mountains of Morocco, *J. Geophys. Res.*, **111**, B03401, doi:10.1029/2005JB003708.
- Mitchum, R. M., Jr., and P. R. Vail (1977), Seismic stratigraphy and global changes of sea level, Part seven: Seismic stratigraphic interpretation procedure, in *Seismic Stratigraphy - Applications to Hydrocarbon Exploration*, edited by C. E. Payton, *Mem. AAPG*, **26**, 135–143.
- Montero, P., F. Haissen, A. El Archi, E. C. Rjimati, and F. Bea (2014), Timing of Archean crust formation and cratonization in the Awsard-Tichla zone of the NW Reguibat Rise, West African Craton: A SHRIMP, Nd–Sr isotopes, and geochemical reconnaissance study, *Precambrian Res.*, **242**, 112–137, doi:10.1016/j.precamres.2013.12.013.
- Moulin, M., D. Aslanian, and P. Unternehr (2010), A new starting point for the South and Equatorial Atlantic Ocean, *Earth Sci. Rev.*, **98**(1–2), 1–37, doi:10.1016/j.earscirev.2009.08.001.

- Olson, P., G. Schubert, C. Anderson, and P. Goldman (1988), Plume formation and lithosphere erosion: A comparison of laboratory and numerical experiments, *J. Geophys. Res.*, *93*(B12), 15,065–15,084, doi:10.1029/JB093iB12p15065.
- Pazzaglia, F., and T. Gardner (1994), Late Cenozoic flexural deformation of the middle US Atlantic passive margin, *J. Geophys. Res.*, *99*(B6), 12,143–12,157, doi:10.1029/93JB03130.
- Persano, C., F. Stuart, P. Bishop, and D. Barford (2002), Apatite (U-Th)/He age constraints on the development of the Great Escarpment on the southeastern Australian passive margin, *Earth Planet. Sci. Lett.*, *200*, 79–90, doi:10.1016/S0012-821X(02)00614-3.
- Potrel, A., J. J. Peucat, C. M. Fanning, B. Auvray, J. P. Burg, and C. Caruba (1996), 3.5 Ga old terranes in the West African Craton, Mauritania, *J. Geol. Soc. London*, *153*, 507–510, doi:10.1144/gsjgs.153.4.0507.
- Ranke, U., U. von Rad, and G. Wissmann (1982), Stratigraphy, facies and tectonic development of the on- and off-shore Aaiun-Tarfaya basin—A review, in *Geology of the Northwestern African Continental Margin*, edited by U. von Rad et al., pp. 86–105, Springer, New York, Berlin, Heidelberg, doi:10.1007/978-3-642-68409-8\_6.
- Ratschiller, L. K. (1968), *Lithostratigraphy of the Northern Sahara*, Museo tridentino di scienze naturali, Trento, Italy.
- Roberts, G. G., and N. White (2010), Estimating uplift rate histories from river profiles using African examples, *J. Geophys. Res.*, *115*, B02406, doi:10.1029/2009JB006692.
- Rosenbaum, G., G. S. Lister, and C. Duboz (2002), Relative motions of Africa, Iberia and Europe during Alpine orogeny, *Tectonophysics*, *359*, 117–129, doi:10.1016/S0040-1951(02)00442-0.
- Ruiz, G. M. H., S. Sebti, F. Negro, O. Saddiqi, D. Frizon de Lamotte, D. Stockli, J. Foecken, F. Stuart, J. Barbarand, and J. P. Schaer (2011), From central Atlantic continental rift to Neogene uplift—western Anti-Atlas (Morocco), *Terra Nova*, *23*, 35–41, doi:10.1111/j.1365-3121.2010.00980.x.
- Sachse, V., R. Littke, S. Heim, O. Kluth, J. Schober, L. Boutib, H. Jabour, F. Perssen, and S. Sindern (2011), Petroleum source rocks of the Tarfaya Basin and adjacent areas, Morocco, *Organic Geochem.*, *42*, 209–227, doi:10.1016/j.orggeochem.2010.12.004.
- Saddiqi, O., F. Z. El Haimer, A. Michard, J. Barbarand, G. M. H. Ruiz, E. M. Mansour, P. Leturmy, and D. Frizon de Lamotte (2009), Apatite fission-track analyses on basement granites from south-western Meseta, Morocco: Paleogeographic implications and interpretation of AFT age discrepancies, *Tectonophysics*, *475*(1), 29–37, doi:10.1016/j.tecto.2009.01.007.
- Sahagian, D. (1988), Epeirogenic motions of Africa as inferred from Cretaceous shoreline deposits, *Tectonics*, *7*(1), 125–138, doi:10.1029/TC007i001p00125.
- Sebti, S. (2011), *Mouvements Verticaux de l'Anti-Atlas Occidental marocain (Kerdous & Ifni): Thermochronologie par traces de fission*, PhD thesis, Univ. Hassan II-Aïn Chock, Casablanca, Morocco.
- Sehrt, M. (2014), *Variscan to Neogene long-term landscape evolution at the Moroccan passive continental margin (Tarfaya Basin and western Anti-Atlas)*, PhD thesis, Ruprecht-Karls-Universität, Heidelberg, Germany.
- Sheridan, R. E., D. L. Musser, L. Glover, M. Talwani, J. I. Ewing, W. Steven Holbrook, G. Michael Purdy, R. Hawman, and S. Smithson (1993), Deep seismic reflection data of EDGE U.S. mid-Atlantic continental-margin experiment: Implications for Appalachian sutures and Mesozoic rifting and magmatic underplating, *Geology*, *21*(6), 563–567, doi:10.1130/0091-7613(1993)021.
- Shuster, D. L., and K. A. Farley (2009), The influence of artificial radiation damage and thermal annealing on helium diffusion kinetics in apatite, *Geochim. Cosmochim. Acta*, *73*, 183–196, doi:10.1016/j.gca.2008.10.013.
- Shuster, D. L., R. M. Flowers, and K. A. Farley (2006), The influence of natural radiation damage on helium diffusion kinetics in apatite, *Earth Planet. Sci. Lett.*, *249*, 148–161, doi:10.1016/j.epsl.2006.07.028.
- Spotila, J. A., G. C. Bank, P. W. Reiners, C. W. Naeser, N. D. Naeser, and B. S. Henika (2004), Origin of the Blue Ridge escarpment along the passive margin of Eastern North America, *Basin Res.*, *16*, 41–63, doi:10.1046/j.1365-2117.2003.00219.x.
- Teixell, A., P. Ayarza, H. Zeyen, M. Fernández, and M. L. Arboleya (2005), Effects of mantle upwelling in a compressional setting: The Atlas Mountains of Morocco, *Terra Nova*, *17*(5), 456–461, doi:10.1111/j.1365-3121.2005.00633.x.
- Turner, J. P., P. F. Green, S. P. Holford, and S. R. Lawrence (2008), Thermal history of the Rio Muni (West Africa)-NE Brazil margins during continental breakup, *Earth Planet. Sci. Lett.*, *270*, 354–367, doi:10.1016/j.epsl.2008.04.002.
- van der Beek, P., S. Cloetingh, and P. Andriessen (1994), Mechanisms of extensional basin formation and vertical motions at rift flanks: Constraints from tectonic modeling and fission-track thermochronology, *Earth Planet. Sci. Lett.*, *121*, 417–433, doi:10.1016/0012-821X(94)90081-7.
- Verati, C., H. Bertrand, and G. Féraud (2005), The farthest record of the Central Atlantic Magmatic Province into West Africa Craton: Precise <sup>40</sup>Ar/<sup>39</sup>Ar dating and geochemistry of Taoudenni basin intrusives (northern Mali), *Earth Planet. Sci. Lett.*, *235*, 391–407, doi:10.1016/j.epsl.2005.04.012.
- Villeneuve, M. (2008), Review of the orogenic belts on the western side of the West African Craton: the Bassarides, Rokelides and Mauritanides, in *The Boundaries of the West African Craton*, edited by N. Ennih and J. P. Liégeois, *Geol. Soc. London Spec. Publ.*, *297*, 169–201, doi:10.1144/SP297.8.
- Villeneuve, M., and B. Marcaillou (2013), Pre-Mesozoic origin and paleogeography of blocks in the Caribbean, South Appalachian and West African domains and their impact on the post “variscan” evolution, *Bull. Soc. Geol. France*, *184*(1–2), 5–20, doi:10.2113/gssgfbull.184.1-2.5.
- von Rad, U., and M. Sarti (1986), Early Cretaceous “events” in the evolution of the eastern and western North Atlantic continental margins, *Geol. Rundsch.*, *75*(1), 139–158, doi:10.1007/BF01770184.
- von Rad, U., and G. Wissmann (1982), Cretaceous-Cenozoic History of the West Saharan Continental Margin (NW Africa): Development, destruction and gravitational sedimentation, in *Geology of the Northwestern African Continental Margin*, edited by U. von Rad et al., pp. 106–131, Springer, New York, doi:10.1007/978-3-642-68409-8\_7.
- von Rad, U., K. Hinz, M. Sarnthein, and E. Seibold (1982), *Geology of the Northwest African Continental Margin*, Springer, Berlin, Heidelberg.
- Voorhoeve, H., and G. Houseman (1988), The thermal evolution of lithosphere extending on a low-angle detachment zone, *Basin Res.*, *1*, 1–9, doi:10.1111/j.1365-2117.1988.tb00001.x.
- Watts, A. B. (2012), Models for the evolution of passive margins, in *Regional Geology and Tectonics: Phanerozoic Rift Systems and Sedimentary Basins*, edited by D. G. Roberts and A. W. Bally, pp. 33–57, Elsevier, Amsterdam.
- Weissel, J. K., and G. D. Karner (1989), Flexural uplift of rift flanks due to mechanical unloading of the lithosphere during extension, *J. Geophys. Res.*, *94*(B10), 13,919–13,950, doi:10.1029/JB094iB10p13919.
- Wissmann, G. (1982), Stratigraphy and Structural features of the continental margin Basin of Senegal and Mauritania, in *Geology of the Northwestern African Continental Margin*, edited by U. von Rad et al., pp. 160–181, Springer, New York, doi:10.1007/978-3-642-68409-8\_9.
- Youbi, N., et al. (2013), The 1750 Ma magmatic event of the West African Craton (Anti-Atlas, Morocco), *Precambrian Res.*, *236*, 106–123, doi:10.1016/j.precamres.2013.07.003.
- Zouhri, S., A. Kchikach, O. Saddiqi, F. Z. El Haimer, L. Baïdier, and A. Michard (2008), The Cretaceous-Tertiary Plateaus in *Continental Evolution: The Geology of Morocco*, *Lect. Notes Earth Sci.*, vol. 116, edited by A. Michard, et al., pp. 331–358, Springer, Berlin Heidelberg, doi:10.1007/978-3-540-77076-3\_7.